NeuroImage: Clinical 25 (2020) 102136

Contents lists available at ScienceDirect

NeuroImage: Clinical

journal homepage: www.elsevier.com/locate/ynicl

Evaluating spatiotemporal microstructural alterations following diffuse traumatic brain injury

Abdalla Z Mohamed[a,1], Frances Corrigan[b,1], Lyndsey E. Collins-Praino[c], Stephanie L. Plummer[d], Neha Soni[a], Fatima A. Nasrallah[a,*]

[a] Queensland Brain Institute, The University of Queensland, Building 79, Upland Road, Saint Lucia, Brisbane, QLD 4072, Australia
[b] Head Injury Laboratory, Division of Health Sciences, University of South Australia, Adelaide, SA 5000, Australia
[c] Cognition, Aging and Neurodegenerative Disease Laboratory (CANDL), Adelaide Medical School, University of Adelaide, Adelaide, SA 5005, Australia
[d] Translational Neuropathology Laboratory, Adelaide Medical School, University of Adelaide, Adelaide, SA 5005, Australia

ARTICLE INFO

Keywords:
Traumatic brain injury
Diffusion tensor Imaging
Structural magnetic resonance imaging
Axonal injury
Neuroinflammation

ABSTRACT

Background: Diffuse traumatic brain injury (TBI) is known to lead to microstructural changes within both white and grey matter detected in vivo with diffusion tensor imaging (DTI). Numerous studies have shown alterations in fractional anisotropy (FA) and mean diffusivity (MD) within prominent white matter tracts, but few have linked these to changes within the grey matter with confirmation via histological assessment. This is especially important as alterations in the grey matter may be predictive of long-term functional deficits.

Methods: A total of 33 male Sprague Dawley rats underwent severe closed-head TBI. Eight animals underwent tensor-based morphometry (TBM) and DTI at baseline (pre-TBI), 24 hours (24 h), 7, 14, and 30 days post-TBI. Immunohistochemical analysis for the detection of ionised calcium-binding adaptor molecule 1 (IBA1) to assess microglia number and percentage of activated cells, β-amyloid precursor protein (APP) as a marker of axonal injury, and myelin basic protein (MBP) to investigate myelination was performed at each time-point.

Results: DTI showed significant alterations in FA and RD in numerous white matter tracts including the corpus callosum, internal and external capsule, and optic tract and in the grey-matter in the cortex, thalamus, and hippocampus, with the most significant effects observed at 14 D post-TBI. TBM confirmed volumetric changes within the hippocampus and thalamus. Changes in DTI were in line with significant axonal injury noted at 24 h post-injury via immunohistochemical analysis of APP, with widespread microglial activation seen within prominent white matter tracts and the grey matter, which persisted to 30 D within the hippocampus and thalamus. Microstructural alterations in MBP + ve fibres were also noted within the hippocampus and thalamus, as well as the cortex.

Conclusion: This study confirms the widespread effects of diffuse TBI on white matter tracts which could be detected via DTI and extends these findings to key grey matter regions, with a comprehensive investigation of the whole brain. In particular, the hippocampus and thalamus appear to be vulnerable to ongoing pathology post-TBI, with DTI able to detect these alterations supporting the clinical utility in evaluating these regions post-TBI.

1. Introduction

Traumatic brain injury (TBI) is a public health epidemic which results from contact and inertial forces acting on the brain (Maas, 2016; Xiong et al., 2013). The resultant cell injury and subsequent neurological dysfunction is caused by both direct physical tissue disruption (primary injury), as well as from delayed molecular and cellular pathophysiological mechanisms that cause progressive white and grey matter damage (secondary injury) (Bramlett and Dietrich, 2004). This secondary injury begins immediately following trauma and may persist for weeks or even years, and is responsible for much of the ongoing neurological impairment post-TBI (Xiong et al., 2013), and may lead to increased amyloid and tau aggregation (Johnson et al., 2013; Mohamed et al., 2018, 2019) causing neurodegenerative disorders (Fann et al., 2018; Kenney and Diaz-Arrastia, 2018).

Diffuse axonal injury (DAI) is one of the most significant

* Corresponding author.
E-mail address: f.nasrallah@uq.edu.au (F.A. Nasrallah).
[1] Co-first authors, equal contribution.

https://doi.org/10.1016/j.nicl.2019.102136
Received 28 October 2019; Received in revised form 12 December 2019; Accepted 13 December 2019
Available online 14 December 2019

consequences of a TBI, taking place in more than 80% of all motor vehicle-induced TBI cases, and is consistently associated with worsened outcome post-injury (Finfer and Cohen, 2001; Maas et al., 2008). Importantly, the majority of axonal damage in TBI is not due to physical tearing of axons at the point of primary injury (Johnson et al., 2013), but due to the initiation of a number of secondary injury processes including influx of calcium, degradation of the cytoskeleton, mitochondrial swelling, oxidative stress, and excitotoxicity which promote progressive axonal injury and eventual axonal swelling and detachment (Blennow et al., 2016; Maas et al., 2008). Axonal injury is both exacerbated by and drives neuroinflammation, with axonal debris activating immune cells (Donat et al., 2017; Witcher et al., 2015).

Diffusion tensor imaging (DTI) which measures the diffusion of water molecules in tissue, can investigate this axonal disruption and its effects on microstructure organization (Mac MacDonald et al., 2007). DTI incorporates fractional anisotropy (FA) that measures the freedom of water diffusion; axial diffusivity (AD) that measures the water diffusion along the fibre orientation; radial diffusivity (RD) that measures the water diffusion in the perpendicular direction to AD; and mean diffusivity (MD), the average of AD and RD (Pierpaoli and Basser, 1996). Numerous studies have shown alterations in FA and MD within prominent white matter tracts including the corpus callosum (CC), internal capsule (IC), and external capsule (EC) following TBI (Bazarian et al., 2007; Hulkower et al., 2013; Inglese et al., 2005; Lepage et al., 2017; Li et al., 2011; Ling et al., 2012; Rubin et al., 2018; Tu et al., 2016; van de Looij et al., 2012; Ware et al., 2017). However, relatively few have linked this to alterations within connected grey matter structures such as the cortex (Budde et al., 2011), hippocampus (Singh et al., 2016), thalamus (Grossman et al., 2012), hypothalamus (Zhou, 2017), and striatum (Shah et al., 2012), and none have examined all regions in the same cohort. Intriguingly, Bouix and colleagues found that those with persistent symptoms post-TBI had the most prominent DTI changes within the grey matter (Bouix et al., 2013), suggesting that detecting pathology within these regions is essential to predicting recovery.

Thus, this study proposes to examine the widespread effects of diffuse TBI on both prominent white and grey matter structures via both DTI and histological analysis on axonal injury, microstructural alterations, and neuroinflammation up to 30 D post-injury. This will provide a key overview of the timeline and spatial distribution of microstructural damage post-TBI.

2. Materials and methods

2.1. Experimental design

This study was approved by the Animal Ethics Committee of the University of Queensland (IRB number: QBI/191/16/MAIC) and the University of Adelaide (M2015-141). Adult male Sprague Dawley rats (10–12 weeks old, 375–425 g, $n = 33$) were purchased from the Animal Resource Centre (Western Australia) and housed under conventional laboratory conditions, with a 12-hour light-dark cycle and access to food and water ad libitum. Eight animals were scanned longitudinally with MRI at baseline (pre-TBI), 24hours (24 h), 7 days (7 D), 14 days (14 D), and 30 days (30 D) post-injury. The remaining animals were perfused at each time point ($n = 5$) for histology, with one cohort of sham animals ($n = 5$ total, 2 24 h and 3 30 D animals).

2.2. Diffuse TBI (weight-drop) injury model

TBI was induced with the Marmarou impact-acceleration model (Marmarou et al., 1994). Animals were initially anaesthetised with 4% isoflurane (mixed air and oxygen 1:0.2) then maintained with 2% isoflurane. An incision was made along the midline of the skull to facilitate the placement of a metal disc centrally between the Lambda and Bregma sutures. TBI animals were placed on a foam bed and TBI induced by releasing a 450 g weight from 2 m onto the metal helmet. All animals were resuscitated using compressed air (0.8 L/min nitrogen; 0.2 L/min oxygen) to avoid aponia which could lead to high mortality rates (Plummer et al., 2018). Successful induction of moderate to severe TBI was assessed 24 h later by rotarod scores < 100, weight reduction of 5–10% and clinical signs (paresis and hunched posture) (Arulsamy et al., 2018).

2.3. Magnetic resonance imaging (MRI) data acquisition

MRI scans were acquired using a 9.4T Bruker Avance III spectrometer (Bruker Biospec, Germany) equipped with a four-element surface rat array coil (Bruker, Germany). Animals were induced with 3% isoflurane (air: oxygen 1:0.8) till fully anesthetised and maintained with 0.1–0.3% isoflurane and a continuous infusion of 0.1 mg/kg/h of dexmedetomidine (Domitor, Germany) with an initial bolus of 0.1 mg/kg. During scans, animals' rectal temperature was maintained at 36 ± 1 °C by a water-circulated heating pad, and respiration continually monitored (70–85 bpm). Following scanning, animals were recovered by an intraperitoneal injection of 0.1 mg/kg of Atipamezole (Antisedan, Germany).

The MRI sequence included a multi-slice, gradient echo pilot scan to optimise positioning within the magnet followed by local shimming to improve the B0 field homogeneity. An anatomical, T2-weighted scan was acquired using a rapid-relaxation-with-enhancement (RARE) sequence with TR/TE = 5900/65 ms, RARE factor = 8, number of averages = 2, FOV = 32 × 25 mm, matrix size = 256 × 256 × 40, and slice thickness = 0.5 mm. DTI was collected using an axial echo-planar imaging (EPI) sequence with TR/TE = 10,000 ms/29 ms, FOV = 24.8 × 24.8 mm, matrix size = 108 × 108 × 41, slice thickness = 0.5 mm, slice gap = 0.1 mm, 32 directions with b-values = 750, 1500s/mm2, and four b0 vol.

2.4. MRI data pre-processing and analysis

Data pre-processing and analysis were performed using the FMRIB Software Library (FSL 5.0.9; https://fsl.fmrib.ox.ac.uk/fsl/fslwiki). DTI and T2 images were reoriented, labels corrected, and T2 corrected for field bias inhomogeneity using N4BiasFieldCorrection (advanced normalization tools (ANTs), Version: 2.1.0-gGIT-N). This was followed by skull stripping performed automatically using 3-D pulse-coupled neural networks (PCNN) (Chou et al., 2011) and corrected manually. Skull-stripped T2 images were co-registered to the Schwarz rat template (Schwarz et al., 2006) linearly and nonlinearly using FMRIB's linear and nonlinear co-registration tool (FLIRT, FNIRT), and the Jacobian maps were determined. To compare tissue volume differences between different time points post-TBI and baseline, tensor-based morphometry (TBM) was calculated based on the Jacobian determinant, which measures the volume changes resulting from the nonlinear registration.

DTI data were corrected for motion using FSL-MCFLIRT (Jenkinson et al., 2002) to realign different volumes to the average of the four b_0 volumes as a reference. The FSL Diffusion Toolkit (Behrens et al., 2003) was used for local fitting of diffusion tensors using a multi-shell approach and to generate the different maps (FA, RD, AD and MD). DTI maps were registered linearly using FLIRT to the T2, then the warp file generated by the T2-to-template normalization was used to register the DTI to the Schwarz rat template.

2.5. Immunohistochemical analysis

Rats were terminally anesthetised with isoflurane and perfused with 10% formalin. Four sections per brain, 5 μm thick, were collected to represent the region −0.5, −1.5, −2.5, and −5 from Bregma. The slides were stained to analyse the microglial response (IBA1 1:1000, 019-19,741, Wako), axonal injury (APP 22C11; Boéhringer, 1:1000) and microstructure (myelin basic protein- MBP: Abcam 1:10,000).

Following dewaxing, endogenous peroxidases were blocked with methanol/hydrogen peroxide (0.5%), followed by antigen retrieval in citrate buffer. Sections were then incubated with 30% normal horse serum for 1 h, prior to incubation overnight with the specific primary antibody. The next day, the appropriate biotinylated secondary antibody (1:250, Vector) was applied for 30 min, followed by streptavidin horseradish peroxidase for 60 min, with the bound antibody detected with 3,3-diaminobenzidine tetrahydrochloride (Sigma). Sections were counterstained with hematoxylin. Slides were digitally scanned using a Nanozoomer, viewed with the associated NDP view software, with images exported for analysis with ImageJ (Arulsamy et al., 2018).

For APP analysis, the full region of the white matter tracts of interest was assessed with all APP + ve lengths and immuno-reactive bulbs counted (Supplementary Table 1). For IBA1 analysis, a 1 mm^2 box was placed in all regions of interest (ROIs) with a few exceptions. For hippocampal analysis, two boxes were used in the −2.5 section and three boxes in the −5 relative to Bregma section to account for the large size of this region. For CC analysis, the region was divided into a left, middle, and right area using the rat brain atlas of Paxinos and Watson and the entire region assessed. These ROIs were used to generate heatmaps. All immuno-reactive cells with clear cell body morphology were counted by a blinded observer. In addition, the morphology of each microglial cell was assessed and characterised as either: ramified (small cell body with multiple fine processes), active (hyper-ramified with an enlarged cell body or an enlarged cell body with reduced processes) or macrophage (rounded, no processes) (Supplementary Figure 1) (Collins-Praino et al., 2018). The number of activated microglia was calculated using the formula:%activated = (number of active and macrophage IBA1 cells/total number of IBA1 + ve cells)*100.

For MBP analysis, a 1mm^2 box was placed within the regions of interest (ROIs) (Supplementary Table 3) and images exported for further analysis via ImageJ as previously described (Van Tilborg et al., 2017). As for the IBA1 analysis of the hippocampus, two boxes were used in the −2.5 section and three boxes in the −5 relative to Bregma section to account for the large size of this region. For CC analysis, a box was placed within the left, middle, and right area based upon the rat brain atlas of Paxinos and Watson and the value averaged. Van Tilborg and colleagues showed that MBP immunostaining provides information about microstructure, with this analysis being sensitive to changes following both neonatal brain injury and adult stroke. The MBP + ve area was determined by manually setting a threshold to include all MBP + ve tissue and then measuring the proportion of the field that was positive. Coherency of myelinated axons was assessed using the `OrientationJ measure' function in ImageJ. Microstructural complexity (fibre length and number of intersections) was measured with the ImageJ plugin DiameterJ, with the number of intersections measured in the grey matter regions only, as the density of fibres within white matter tracts interferes with this analysis (Van Tilborg et al., 2017). Images were first segmented by removing the background, a threshold applied to include all the MBP + ve staining and noise removed, before measurement with DiameterJ.

2.6. Statistical analysis

2.6.1. Neuroimaging

Voxel-based analysis was used to investigate the temporal profile of the microstructural changes following TBI to 30 D post-injury as compared to baseline. The data were fed into voxel-wise cross-subject statistics by repeated-measures analysis of variance (ANOVA) to observe the main effect of time post-TBI followed by a post-hoc analysis using paired t-tests to identify the significant differences between the different time points and baseline. The analysis was done using a non-parametric permutation test with FSL-randomise (Nichols and Holmes, 2002) with 5000 permutations. The results were corrected for multiple comparisons using family wise error (FWE; $p < 0.05$), with the minimum cluster size of 100 voxels.

Furthermore, we performed an ROI analysis by extracting the values of DTI parameters from several ROIs, including the CC, IC, EC, cortex, thalamus, and hippocampus which were segmented using an atlas-based approach based on the Schwarz template (Schwarz et al., 2006). The values of the Jacobian co-efficient for the posterior-dorsal hippocampus, the subiculum hippocampus, and the thalamus, multiplied by the size of the masque were used to estimate the individual regional volumes. The ROI data were analysed using one-way ANOVA with repeated measures by R-Studio (version 3.3.1; R Foundation for Statistical Computing, Vienna, Austria). Bonferroni correction was used to correct for multiple comparisons ($p < 0.05$).

2.6.2. Immunohistochemistry

The ROIs assessed at the different levels Bregma −0.5, −1.0, −2.5, −5 were averaged to determine a mean level of expression for each structure (e.g., cortex, hippocampus). A two-way ANOVA was then performed, with Tukey post-hoc testing with Bonferroni correction for multiple comparisons as required, with the significance level set at 0.05.

3. Results

Following TBI, animals experienced brief seizures (< 15 s) observed by either tail twitching or generalised seizures immediately after the impact.

3.1. Temporal changes in brain volume following TBI

A significant increase in regional volume was observed in the striatum at 7 D (mean ± std = 116.12 ± 8.41; $p < 0.01$), 14 D (107.26 ± 6.76; $p = 0.05$), and 30 D (110.79 ± 5.96; $p = 0.01$) as compared to baseline (99.71 ± 3.75) and thalamus at 24 h (73.1 ± 3.78; $p < 0.01$), 7 D (71.65 ± 2.14; $p = 0.04$), 14 D (70.85 ± 2.03; $p = 0.02$), and 30 D (75.76 ± 4.75; $p < 0.01$) as compared to baseline (68.02 ± 2.06). On the other hand, a significant reduction in the volume of the posterior dorsal hippocampus was seen at 7 D (38.6 ± 1.8; $p = 0.05$), 14 D (38.44 ± 1.56; $p = 0.05$), and 30 D (37.82 ± 1.69; $p = 0.02$) as compared to baseline (41.05 ± 2.12); and further reduced volume in the subiculum hippocampus at 14 D (20.72 ± 0.95; $p < 0.01$), and 30 D (20.85 ± 1.16; $p < 0.01$) as compared to baseline (23.21 ± 1.37); (Fig. 1). Ventricular volume was increased at 24 h (13.25 ± 1.37; $p = 0.01$) and 7 D (12.01 ± 1.10; $p = 0.05$) post-TBI compared to baseline (10.53 ± 1.54) then returned to baseline at 14 D (10.72 ± 1.77). (Fig. 1B).

3.2. Alterations in FA, RD, AD and MD following TBI over time as compared to baseline

FA values were significantly higher in the white matter at 7 D mainly in the body of the CC (CCb), optic tract (OP), and EC compared to baseline. An increase in FA was also seen at 14 D in the genu of CC (CCg), OP, CCb, splenium of CC (CCs), IC, and EC (Fig. 2A) and at 30 D in the CCg, OP, CCb, CCs, IC, and EC. No white-matter FA changes were observed at 24 h (Fig. 2A). In the grey matter; however, a reduction in FA values was seen in the cortex at 24 h and 30 D, while increases were seen in the thalamus at 7 D, in the amygdala, thalamus, and hippocampus at 14 D, and in the thalamus and hippocampus at 30 D (Fig. 2A).

RD values were significantly reduced in both the grey matter and white matter post-TBI compared to baseline. In the white matter, RD was reduced at 24 h in OP and CCs, at 7 D in the hippocampal commissure (HCC), anterior commissure (AC), EC, OP, and IC, at 14 D in the CCg, CCb, CCs, IC, EC, OP, HCC, and AC, and at 30 D in the CCg, OP, CCb, CCs, IC, and EC (Fig. 2B). In the grey matter, RD was reduced in the thalamus and amygdala at 24 h, in the caudate-putamen (CPu), thalamus, and hippocampus at 7 D, in the cortex, amygdala, thalamus,

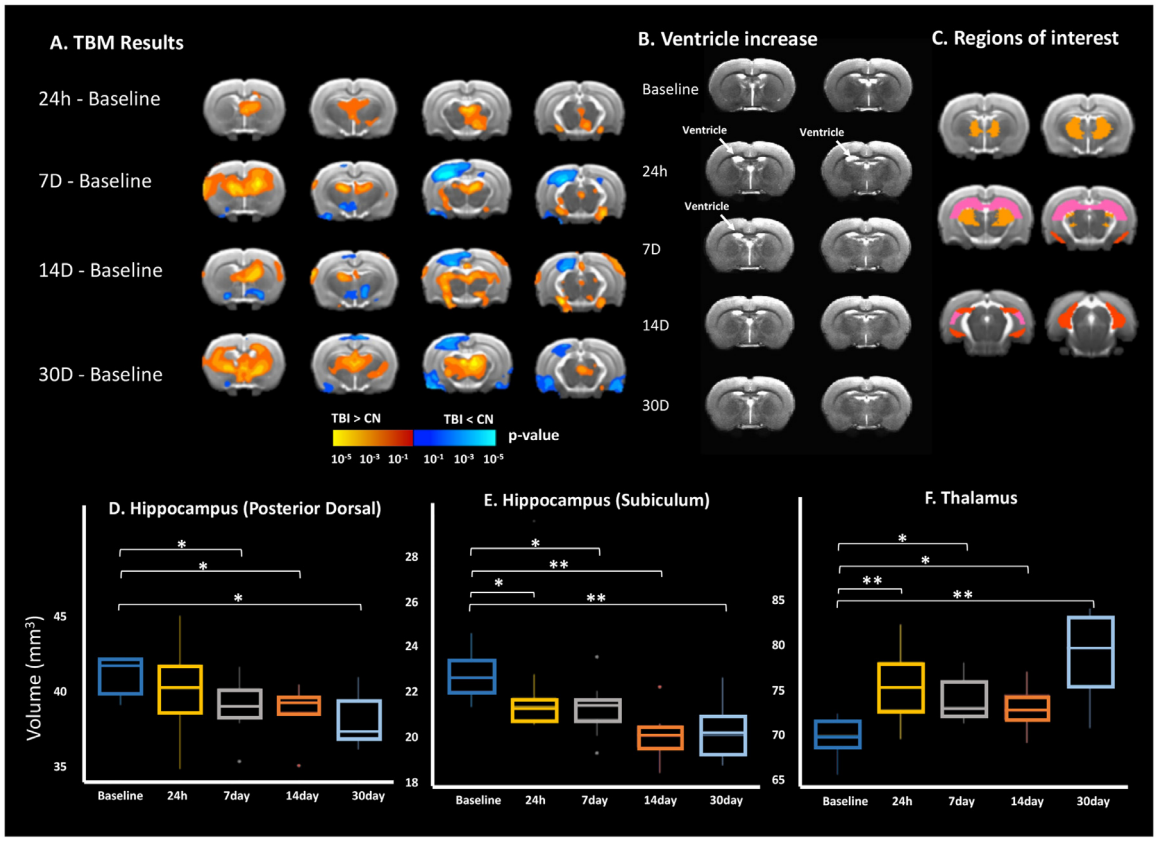

Fig. 1. Brain volume changes following TBI. It shows the different results of (A) the tensor-based morphometry, (B) representing group average of the T2 images showing increased ventricle size at 24 h, and 7days with recovery at 14 D and 30 D post-TBI, (C) ROI schematic showing regions used to calculate the box-plots in (D-F) including (D) posterior-dorsal hippocampus (in pink), (E) subiculum hippocampus (in red), and (F) thalamus (in brown).

and hippocampus at 14 D, and in the hippocampus at 30 D (Fig. 2B).

In contrast to baseline, we observed no changes in AD in CC, but decreased AD values were seen in the OP and HCC at 24 h, 7 D, and 14 D, and in the IC at 24 h and 7 D (Supplementary Figure 2). Furthermore, reduced AD values were observed in the cortex at 24 h, 14 D, and 30 D, in the hippocampus at 14 D, and in thalamus at 24 h and 7 D (Supplementary Figure 2A). MD was decreased in the white matter in the OP at 24 h, in OP, HCC, and IC at 7 D, and in OP, CCb, and HCC at 14 D, with no white-matter changes at 30 D (Supplementary Figure 1B). MD was further decreased in the hippocampus and thalamus at 24 h, in the amygdala, and cortex at 7 D, in the amygdala, and cortex at 14 D, and in the cortex at 30 D (Supplementary Figure 2B).

Using ROI analysis, similar changes were observed where FA values were increased in the CC at 7 D ($p = 0.04$), 14 D ($p = 0.02$), and 30 D ($p = 0.02$), with no differences at 24 h ($p = 0.06$); in EC at 7 D ($p < 0.001$), 14 D ($p < 0.001$), and 30 D ($p = 0.004$) with no differences at 24 h ($p = 0.4$); in IC at 7 D ($p < 0.001$), 14 D ($p < 0.001$), and 30 D ($p = 0.004$) with no differences at 24 h ($p = 0.08$); in the hippocampus at 14 D ($p = 0.03$) with no differences at the other timepoints; and in the thalamus at 7 D ($p = 0.005$), and 14 D ($p < 0.001$). We observed no differences in the cortex ($p = 0.5$) (Fig. 2C).

Similarly, our ROI analysis of the RD values showed reduced RD in the CC at 14 D ($p < 0.001$) and 30 D ($p = 0.05$); in EC at 7 D ($p = 0.01$) and 14 D ($p < 0.001$); in IC at 14 D ($p = 0.01$); in the cortex at 14 D ($p < 0.01$); in the hippocampus at 7 D ($p = 0.04$) and 14 D ($p < 0.001$); and in the thalamus at 24 h (p 0.03), 7 D ($p = 0.04$), and 14 D ($p = 0.008$) (Fig. 2D).

MD was further decreased in the hippocampus and thalamus at 24 h, amygdala, and cortex at 7 D, in the amygdala, and cortex at 14 D, and in the cortex at 30 D (Supplementary Figure 2).

3.3. Axonal injury assessment post-TBI using APP

Representative images of APP staining, with semi-quantification of the number of APP + ve immunoreactive bulbs and lengths can be seen in Fig. 3, with a heat map representation of the white matter tracts of interest are shown in Fig. 4. Overall, the levels of APP staining revealed axonal injury in several white-matter tracts at 24 h which were resolved at 7 D, with a slight increase again at 14 D. Two-way ANOVA found a significant interaction ($F_{(48.260)} = 16.6$, $p < 0.0001$), with a significant main effect of time-post-injury ($F_{(12,260)} = 52.84$, $p < 0.0001$) and brain region ($F_{(4260)} = 76.64$, $p < 0.0001$). Post-hoc analyses found significant increases in APP + ve lengths and bulbs at 24 h within the CC (131 ± 60.07 vs. 6 ± 3.5, $p < 0.0001$), cingulum (73 ± 16.12 vs. 2.8 ± 1.10, $p < 0.0001$), OP (111.4 ± 26.72 vs. 6 ± 2.45, $p < 0.0001$) and cerebral peduncle (25 ± 15.92 vs. 2.6 0.54, $p < 0.01$), with no significant differences noted in any other white matter tract examined (Fig. 3B). The levels then decreased within all these regions such that the levels at 24 h were significantly higher than at 7 D, 14 D, or 30 D post-injury (Fig. 3B). Notably, within the CC (26 ± 17.23 vs. 6 ± 3.5, $p < 0.05$), cingulum (24.6 ± 19.12 vs. 2.8 ± 1.10, $p < 0.01$) and OP (29.2 ± 6.15 vs. 6 ± 2.45, $p < 0.01$), numbers of APP + ve lengths and bulb were again significantly higher than shams at 14 D post-injury, but not at 30 D post-injury (CC $p = 0.74$, cingulum $p = 0.80$, OP $p = 0.87$) (Fig. 3B).

3.4. Microglial activity after TBI

Representative images of IBA1 immunoreactivity are presented in Fig. 5A, with analysis of the number of IBA1 + ve cells (5B),% microglial activated (5C), as well as a representative heat map (Fig. 6). Assessment of microglial number found a significant interaction ($F_{(28,160)} = 1.941$,

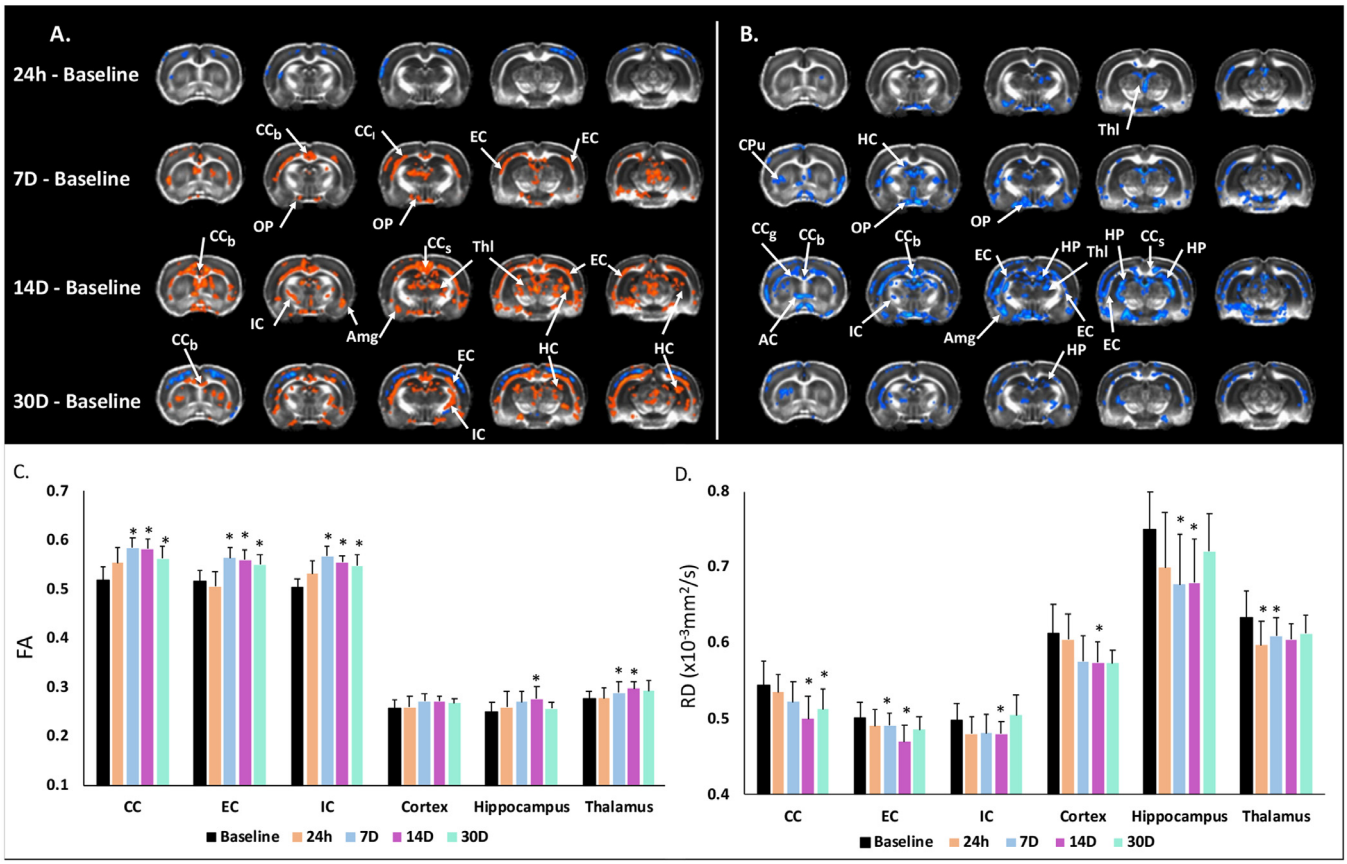

Fig. 2. Longitudinal diffusion tensor imaging (DTI) reveals altered white- and grey-matter microstructures over one-month following TBI. (A) Voxel-wise comparison of FA values and (B) RD values between TBI time points (i.e. 24 h, 7 D, 14 D, and 30 D post-TBI) and the baseline time point (each row) at different slice positions (columns). Yellow-red indicates TBI > Baseline, and blue-light blue indicates TBI < Baseline. (C) shows the FA values in four ROIs and (D) shows the RD values at the same ROIs. OP, optic tract; CCb, the body of the corpus callosum; CCl, lateral corpus callosum; CCg, genu of corpus callosum; CCs, splenium of corpus callosum; IC, internal capsule; EC, external capsule, pF, piriform cortex; Thl, thalamus; Amg, amygdala; HP, hippocampus; * $P < 0.05$.

$p < 0.01$) with main effects of both time-post-injury ($F_{(7160)} = 4.52$, $p < 0.01$) and brain region ($F_{(7160)} = 11.24$, $p < 0.0001$). Post-hoc analyses found a significant increase within the CC at 7 D (49.35 ± 11.54, $p < 0.001$), 14 D (53.3 ± 7.00, $p < 0.0001$), and 30 D post-injury ($p < 0.0001$) relative to sham (33.22 ± 2.83), but not at 24 h (42.00 ± 6.43, $p = 0.17$) (Fig. 5B). An increase was similarly seen in the other white matter region assessed in the optic tract, reaching significance at 14 D post-injury (43.87 ± 4.25 vs. 30.65 ± 2.45, $p < 0.01$). No difference in any of the grey matter regions assessed (cortex, striatum, hippocampus, thalamus, hypothalamus, midbrain) was noted at any time-point post-injury (Fig. 5B).

Significant differences depending on the anatomical region assessed were also found for microglial activation (Fig. 5C, Fig. 6). Two-way ANOVA found a significant interaction $F_{(28,160)} = 3.122$, $p < 0.001$ with main effects of both time-post-injury ($F_{(7160)} = 45.61$, $p < 0.0001$) and brain region ($F_{(7160)} = 62.42$, $p < 0.001$). At 24 h post-injury, significantly higher amounts of microglia activation relative to sham were seen in the cortex (26 ± 9.7 vs. 3.72 ± 1.28, $p < 0.001$), thalamus (37.49 ± 8.28 vs. 7.08 ± 2.61, $p < 0.001$), hippocampus (42.48 ± 15.66 vs. 9.17 ± 2.65, $p < 0.0001$), hypothalamus (29.77 ± 10.60 vs. 3.7 ± 1.31, $p < 0.0001$), midbrain (23.03 ± 5.50 vs. 9.40 ± 1.01, $p < 0.05$), CC (65.88 ± 10.24 vs. 12.13 ± 3.5, $p < 0.0001$) and OP (41.69 ± 8.65 vs. 10.74 ± 3.56, $p < 0.0001$), but not the striatum, where no increase in activated microglia was noted at any time-point post-injury (12.16 ± 8.12, 7.54 ± 1.95, 12.06 ± 4.37, and 9.13 ± 3.37 at 24 h, 7 D, 14 D, and 30 D post-injury respectively vs. 3.84 ± 2.91 in shams) (Fig. 5C). A rapid return to sham levels was seen in the cortex, with no further significant differences relative to sham out to 30 D post-injury ($p = 0.81$, 0.58, and 0.46 at 7, 14, and 30 D post-injury, respectively) (Fig. 5C). In contrast, within the thalamus, hippocampus, CC, and OP, although the levels had decreased at the 7 D, 14 D, and 30 D time-points, such that they were significantly different to the 24 h time-points ($p < 0.05$), the levels remained significantly higher relative to sham animals out to 30 D post-injury. Within the midbrain and hypothalamus, no significant differences were noted at 7 D (20.71 ± 10.53 vs. 9.40 ± 1.0, $p = 0.11$) and 7 D and 14 D post-injury (12.18 ± 3.62 and 13.31 ± 4.6 vs. 3.7 ± 1.31, $p = 0.37$ and 0.24, respectively) relative to sham animals, with a significant increase than seen at 14 D and 30 D in the midbrain (25.68 ± 6.70 and 22.34 ± 4.93, $p < 0.01$, $p < 0.05$, respectively) and at 30 D only in the hypothalamus (17.42 ± 3.25, $p < 0.05$) (Fig. 5C).

3.5. Myelination and microstructure after TBI

Myelination and, hence, microstructure post-TBI were assessed via immunohistochemical analysis of MBP staining (Fig. 7). Two-way ANOVA of the%area of MBP staining found a trend towards a significant interaction (F32180 = 1.45, $p = 0.07$), with significant main effects of time-post-injury (F4180 = 6.93, $p < 0.0001$) and brain region assessed (F8180 = 11.06, $p < 0.0001$). Post-hoc analyses found no significant differences at any time-point post-injury within the cortex, CC, striatum, hypothalamus, hippocampus, thalamus, midbrain, or OP. Some variability was noted within the cerebral peduncle, with higher levels relative to sham (38.81 ± 3.10) at 24 h (46.41 ± 4.43, $p = 0.11$) and 30 D (46.69 ± 0.80, $p = 0.08$), although this was not significant.

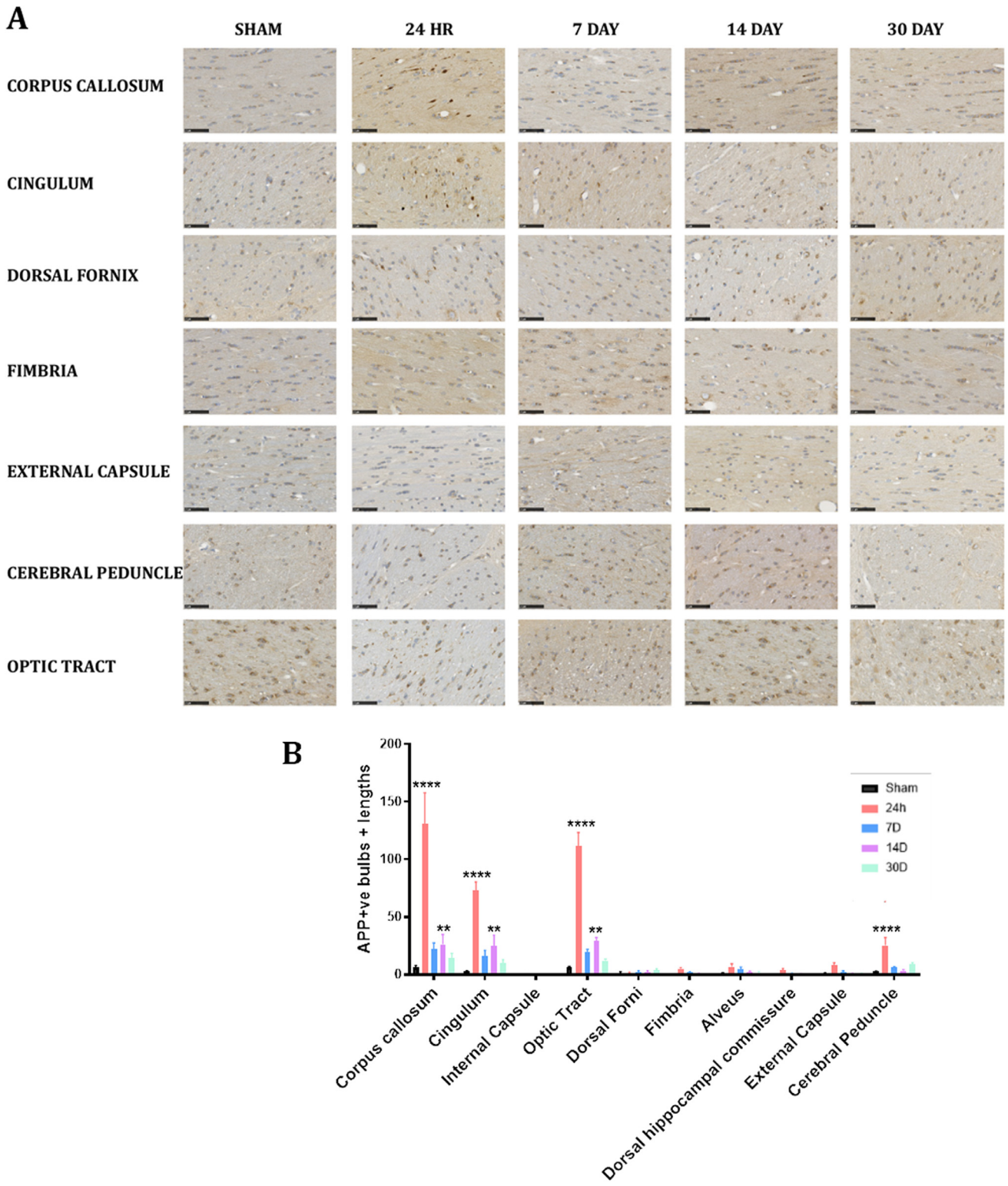

Fig. 3. Representative images of APP immunohistochemistry from our regions of interest. Scale bar = 50 μm (A), with counts of the total number of APP + ve lengths and bulbs (B), * indicates significantly different compared to sham (* = $p < 0.05$; ** = $p < 0.01$: *** = $p < 0.001$).

However, levels at 24 h and 30 D were significantly higher than at 7 D post-injury (35.55 ± 7.68, $p < 0.05$) (Fig. 7B, Table 1).

Examination of coherence of the MBP + ve fibres found a significant interaction (F32180 = 3.585, $p < 0.0001$), with significant main effects of time-post-injury (F4180 = 5.928, $p < 0.0001$) and brain region assessed (F8180 = 28.61, $p < 0.0001$). Coherence of fibres was decreased within the cortex following injury, with this reaching significance at 14 D (0.07 ± 0.09 vs. 0.11 ± 0.02, $p < 0.05$) and 30 D (0.07 ± 0.01 vs. 0.11 ± 0.02, $p < 0.05$). A similar pattern was seen within the thalamus, with significant decreases relative to sham (0.10 ± 0.03) noted at 7 D (0.06 ± 0.01, $p < 0.05$), 14 D (0.06 ± 0.02, $p < 0.05$) and 30 D post-injury (0.06 ± 0.01, $p < 0.05$). No changes were noted within the striatum, hippocampus, hypothalamus, or midbrain at any time-point post-injury. Within the white matter tracts examined, coherence was

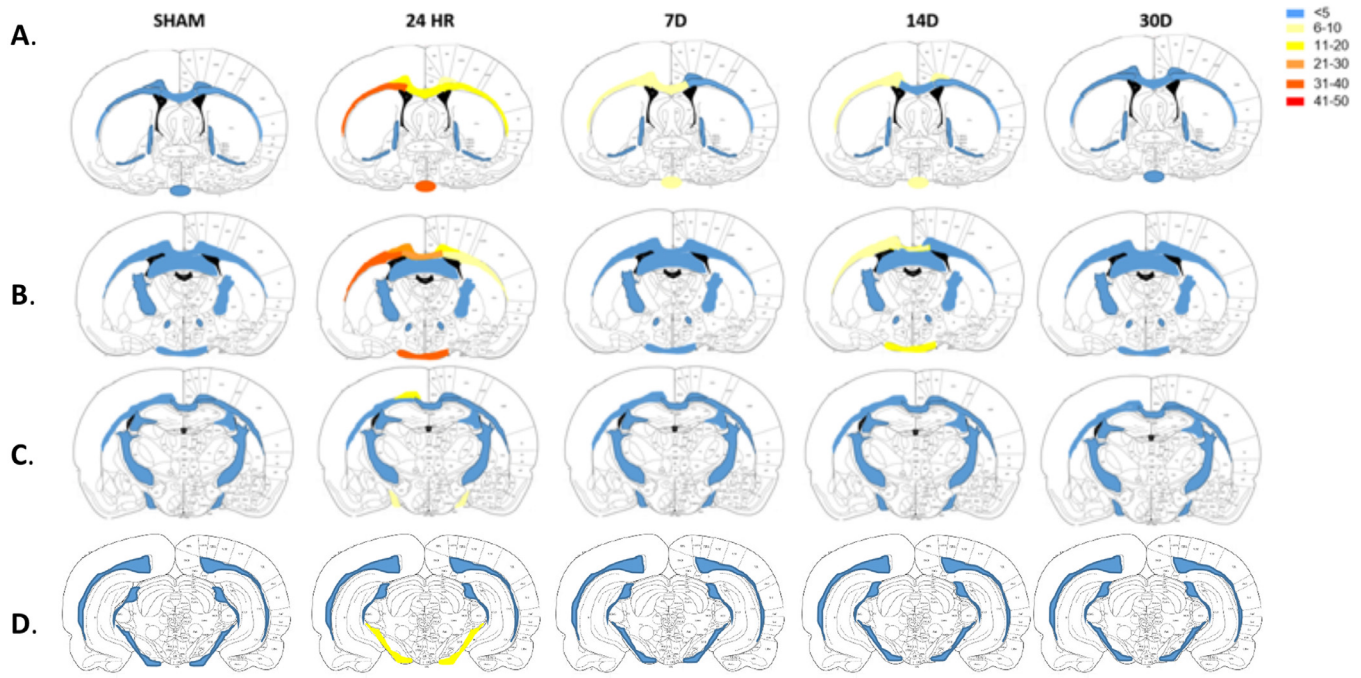

Fig. 4. Heat map representation of the number of APP + ve immunoreactivity bulbs and lengths counted in each of the white matter tracts of interest. Value calculated as the average of $n = 5$.

increased at 24 h (CC 0.20 ± 0.02 vs. 0.12 ± 0.01, $p < 0.001$, cerebral peduncle 0.09 ± 0.05 vs. 0.05 ± 0.01, $p < 0.05$, and OP 0.11 ± 0.02 vs. 0.06 ± 0.02, $p < 0.05$), with no differences relative to sham noted at any other time-point post-injury (Fig. 7C, Table 1). Two-way ANOVA of the total length of MBP + ve fibre staining found a significant interaction ($F32180 = 1.566$, $p < 0.05$), with significant main effects of time-post-injury ($F4180 = 4.934$, $p < 0.001$) and brain region assessed ($F8180 = 66.02$, $p < 0.0001$). Post-hoc analyses found minor differences in the CC, with lower values at 7 D compared to 24 h (22,870.3 ± 5433.62 vs. 29,098.5 ± 3145.41, $p < 0.05$) and 30 D post-injury (29,175.3 ± 892.77, $p < 0.05$), but not sham animals (25,336.8 ± 10,124.89, $p = 0.77$). In the hippocampus, the total length was higher at 30 D than at 14 D (36,860.4 ± 5092.71 vs. 30,181.4 ± 2048.1, $p < 0.05$), but not relative to shams (32,626.8 ± 3702.55, $p = 0.28$). In the cerebral peduncle, the total myelin basic protein fibre length was higher at 14 D compared to sham (38,255 ± 5253.33 vs. 30,858.2 ± 1434.98, $p < 0.01$), but not at any other time point: 24 h (35,995 ± 1730.33, $p = 0.12$), 7 D (34,788 ± 5808.17, $p = 0.35$), and 30 D post-injury (35,632.3 ± 3679.1, $p = 0.18$) (Fig. 7D, Table 1).

The number of intersections as a measure of complexity was only measured in grey matter regions with a significant interaction ($F20120 = 1.87$, $p < 0.05$) and significant main effects of time post-injury ($F4120 = 11.27$, $p < 0.0001$) and the brain region assessed ($F5120 = 33.29$, $p < 0.0001$) noted. Post-hoc analyses found a significant decrease in the number of intersections within the cortex at 24 h compared to sham animals (3890.33 ± 290.13 vs. 4859.12 ± 450.95, $p < 0.05$), which had recovered by 30 D such that the levels were significantly higher at this time point than at 24 h (4976.46 ± 503.78 vs. 3890.33 ± 290.13, $p < 0.05$). A similar pattern was seen within the thalamus, with a significant decrease seen at 7 D post-injury relative to sham (4055.5 ± 400.14 vs. 5384.08 ± 551.03, $p < 0.05$), with a trend towards a decrease at 14 D (4515.71 ± 509.22, $p = 0.08$) but no difference at 30 D (4749.63 ± 161.36, $p = 0.35$). In contrast, within the hippocampus, no difference was seen at 24 h (3908.16 ± 525.19, $p = 0.85$), 7 D (3875.85 ± 275.46, $p = 0.95$) or 14 D (3343.74 ± 290.84, $p = 0.89$) relative to sham (3646.42 ± 412.55), but a significant increase was seen at 30 D post-injury (4714.07 ± 770.66, $p < 0.01$) (Fig. 7E, Table 1). No differences were seen within the hypothalamus, striatum, or midbrain at any time-point post-injury (Table 1).

4. Discussion

This work utilises DTI and histology to investigate regional specific microstructural alterations following a single moderate-severe TBI from 24 h to 30 D post-injury. Extensive alterations were noted within white matter tracts, with increased FA, reduced RD, AD, and MD in the CC, IC, EC, and OP, peaking at 14 D post-TBI. Alterations were also seen in the grey matter, with decreased MD, AD, and RD within the cortex, hippocampus and thalamus. In the cortex, reduced FA values were noted, while increased FA was seen in the thalamus and hippocampus. Immunohistochemical analysis supported the presence of extensive axonal injury, with levels of APP, a measure of impaired axonal transport, peaking at 24 h post-injury. Examination of myelinated fibres through MBP immunostaining revealed subtle alterations acutely within white matter tracts and sub-acutely within the cortex, thalamus and hippocampus. Ongoing neuroinflammation, as assessed by number of activated microglia, was prominent within the CC and OP where axonal injury levels were highest and persisted to 30 D post-injury. Within the grey matter, the cortex, hypothalamus, thalamus, hippocampus, and midbrain demonstrated increased microglial activation at 24 h, which similarly persisted to post- injury within the thalamus, hippocampus, and midbrain. There were minimal changes in the overall microglia number, suggesting that this was due to activation of local microglia/macrophages rather than overall recruitment.

In line with previous findings (Tu et al., 2016; van de Looij et al., 2012), we observed an increase in ventricle size at 24 h and 7 D, with a return to baseline at 14 D post-TBI. Such increases in ventricle size are consistent with clinical studies of TBI (Gale et al., 1995; Zhao et al., 2014). Prominent changes were noted on DTI in the white matter tracts including the CC, IC, EC and OP. In healthy axons, diffusion is constrained by the microstructural organization, with water diffusing freely parallel to axons, but restricted in other directions, with this

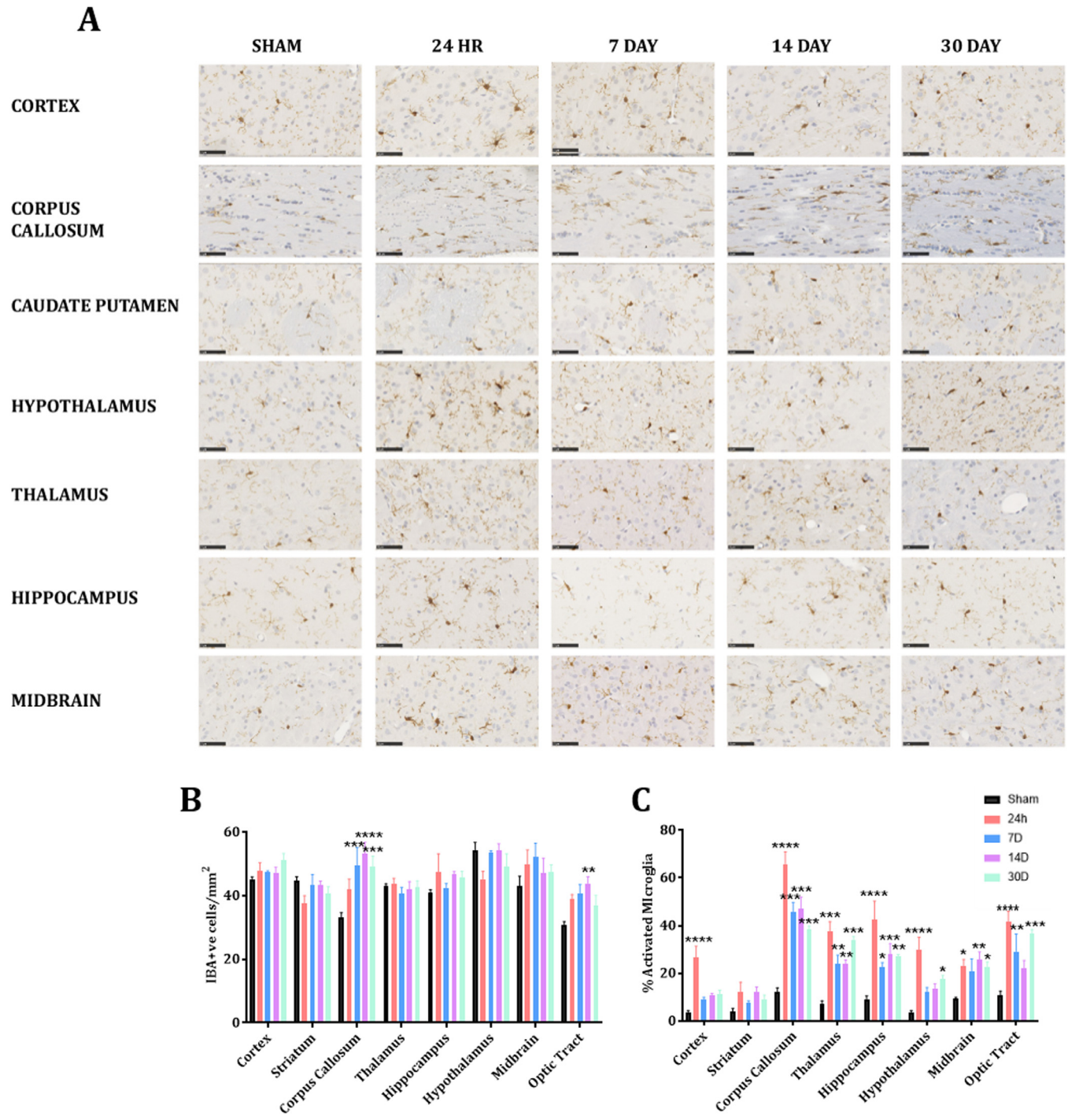

Fig. 5. Representative images of IBA1 immunohistochemistry from our regions of interest. Scale bar = 50 μm. Image representative of $n = 5$ per group (A), with counts of the number of IBA1 + ve cells/mm2 (B) and% activated microglia (C). * indicates significantly different compared to sham (* = $p < 0.05$; ** = $p < 0.01$: *** = $p < 0.001$); # indicates significantly different compared to 24 h (# = $p < 0.05$; ## = $p < 0.01$; ### = $p < 0.001$).

asymmetry known as anisotropic diffusion (FA). MD, in contrast, refers to the total diffusion of water in a voxel, measured either as parallel (AD) or perpendicular (RD) to the fibres. The FA increases noted in the CC have been reported in previous clinical studies (Bazarian et al., 2007; Ling et al., 2012; Mayer et al., 2010), with reduced MD and RD also reported in the CC up to 7 D post-injury following TBI (Li et al., 2011; Singh et al., 2016). The decrease in MD observed may also be driven by the increase in glial number (Budde et al., 2011), in line with the increase in IBA1 + ve cells within the white matter tracts examined. Factors found to be associated with increased FA include increased myelination, increased axon density and increased coherence, although this is a simplification, given that the role of glia and blood vessels are not considered (Scholz et al., 2014). Here, increased coherence was seen via histological examination of the MBP + ve fibres within the white matter tracts at 24 h post-injury, which can lead to increased FA, by decreasing fibre dispersion, and thus, facilitating water movement in a single direction (Chang et al., 2017). Increased coherence of white matter tracts may be caused by increases in axonal intracellular water relative to the extracellular space with reduced RD, as reported here, causing increased FA due to the more tightly compacted axons

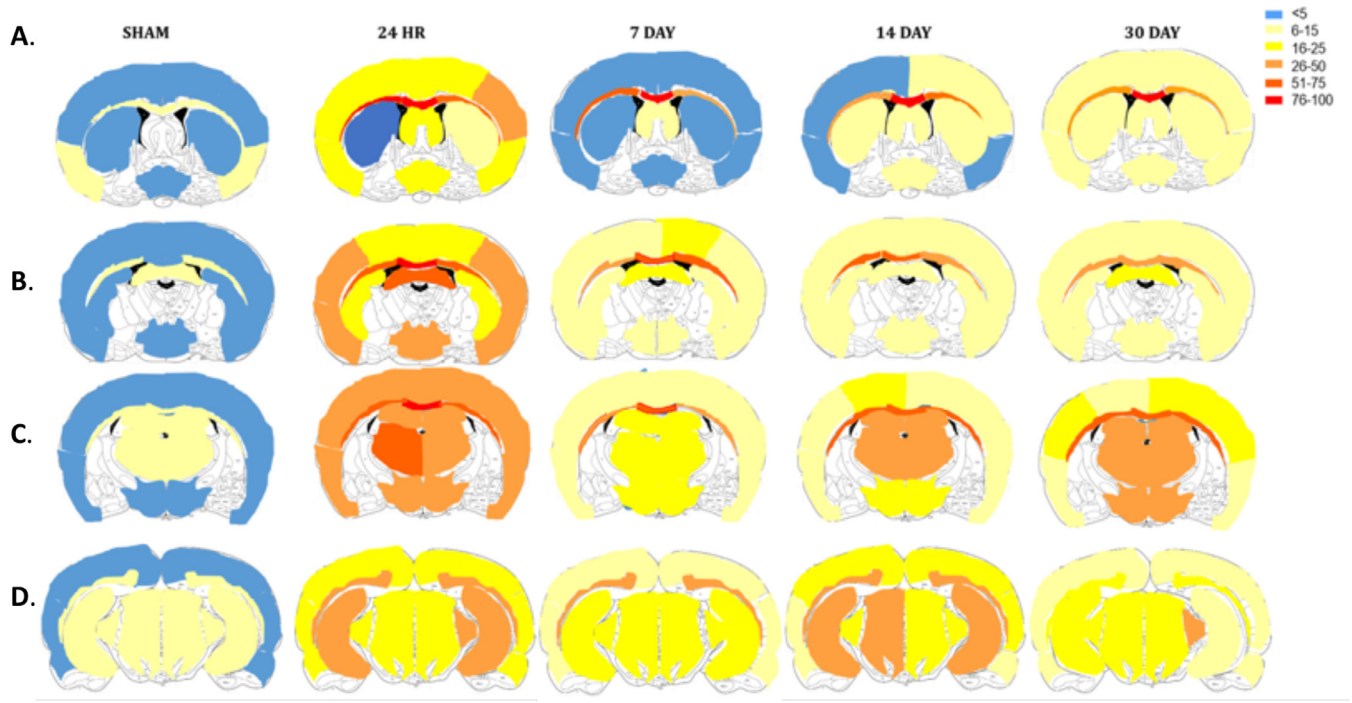

Fig. 6. Heat map representation of the% activated microglia within our areas of interest. Values calculated as the average of $n = 5$ per group.

(Rosenblum, 2007; Sotak, 2002). Modelling studies suggest that even small departures from the normal distribution of intracellular and extracellular water can lead to dramatic changes in perpendicular diffusion coefficients (Peled, 2007). Of note, the histological detection of increased coherence at 24 h differed to the alterations in DTI metrics, which peaked at 14 D post-injury. It should be noted that DTI, although highly sensitive, is not specific, as numerous factors can affect the degree of anisotropy including factors related to axons themselves (axon diameter, inter-axon spacing, water content, crossing of fibres, myelination), as well as the external environment, including the number and activation state of glial cells (Tournier et al., 2011). Hence the interplay of numerous factors leads to the overall change in DTI metrics, making it difficult to determine the underlying cause, and thus caution must be taken when interpreting DTI results.

Indeed, it should also be noted that these findings are in contrast to a number of other pre-clinical and clinical studies where decreased FA and increased MD are reported within white matter tracts, including the CC and IC in the subacute phase post-TBI (Arfanakis et al., 2002; Budde et al., 2011; MacDonald et al., 2007; Matsushita et al., 2011; Tu et al., 2016; van de Looij et al., 2012). Indeed, when white matter is damaged, diffusion is thought to become less symmetric, leading to decreases in FA due to degenerative changes, such as Wallerian degeneration, axonal collapse and myelin degradation (Wallace et al., 2018). Pre-clinical studies reporting these contrasting DTI findings include those employing the same diffuse TBI model employed here (Tu et al., 2016; van de Looij et al., 2012), as well as the mixed focal and diffuse injury induced via lateral fluid percussion (LFPI) (Johnstone et al., 2015; Wright et al., 2016) and focal injury via controlled cortical impact (CCI) (Budde et al., 2011; MacDonald et al., 2007), suggesting that this is not specific to injury type. Nonetheless, our injury appears less severe than the same weight drop model employed by Tu colleagues, where MBP staining was decreased at 10 D post-injury (Tu et al., 2016) compared to our findings where there were no alterations in expression of MBP, suggesting that our model did not cause widespread demyelination of the white matter tracts nor cause loss of myelinated axons. Similarly, as per the nature of the insult, both LFPI and CCI lead to extensive cell loss with widespread axonal degeneration within white matter tracts such as the CC and IC, as well as the cerebral cortex, hippocampus, and thalamus (Corrigan et al., 2011). Indeed, in focal CCI injury, MBP levels within the CC detected via western blot were decreased acutely (within the first week) (Glushakova et al., 2014; Ming et al., 2006), with this persisting out to one-year post-injury (Loane et al., 2014). Therefore, more subtle alterations may be occurring within this diffuse injury model, including fragmentation, decompaction, or separation of the myelin from the axon, which would require confirmation with electron microscopy studies (Armstrong et al., 2016; Taib et al., 2017).

Nonetheless widespread axonal injury was detected via APP immunohistochemistry within the CC, cingulum, OP, EC, and cerebral peduncle. APP staining identifies axons with impaired axonal transport (Otsuka et al., 1991), as APP is normally transported by the fast mode of anterograde axoplasmic transport and rapidly pools at sites of impaired transport (Smith et al., 2003). APP accumulation peaked at 24 h, before decreasing, in line with previous reports using this model of TBI (Hellewell et al., 2010). A small increase was again seen at 14 D within the CC, cingulum, and OP suggestive of ongoing pathology which was supported by findings of persistent inflammation within these regions. The cingulum and CC are proposed to be particularly vulnerable to injury (Dikranian et al., 2008) Indeed, the original publication of the impact-acceleration model noted massive DAI within the CC, IC, OP, cerebral, and cerebellar peduncles (Foda and Marmarou, 1994).

This axonal injury appeared to drive ongoing pathology, with increased microglial activation within the CC and OP to 30 D post-injury, particularly in the more anterior section examined, which are more directly under the impact site. The time-line of DTI changes was different with no differences seen at 24 h, maximal changes at 14 D post-injury, with persistence to 30 D. This may relate to ongoing axonal injury that was not fully appreciated via APP immunohistochemistry, as impaired axonal transport is only one marker of axonal injury. Neurofilament compaction, where interfilament spacing is reduced due to side-arm phosphorylation or proteolysis, is another key component of axonal injury (Siedler et al., 2014), with evidence to suggest that neurofilament compaction may occur in different subpopulations of axons to those showing impaired axonal transport (DiLeonardi et al., 2009). Thus, changes noted on DTI may relate to ongoing cytoskeletal damage within axons causing microstructural alterations, not detected

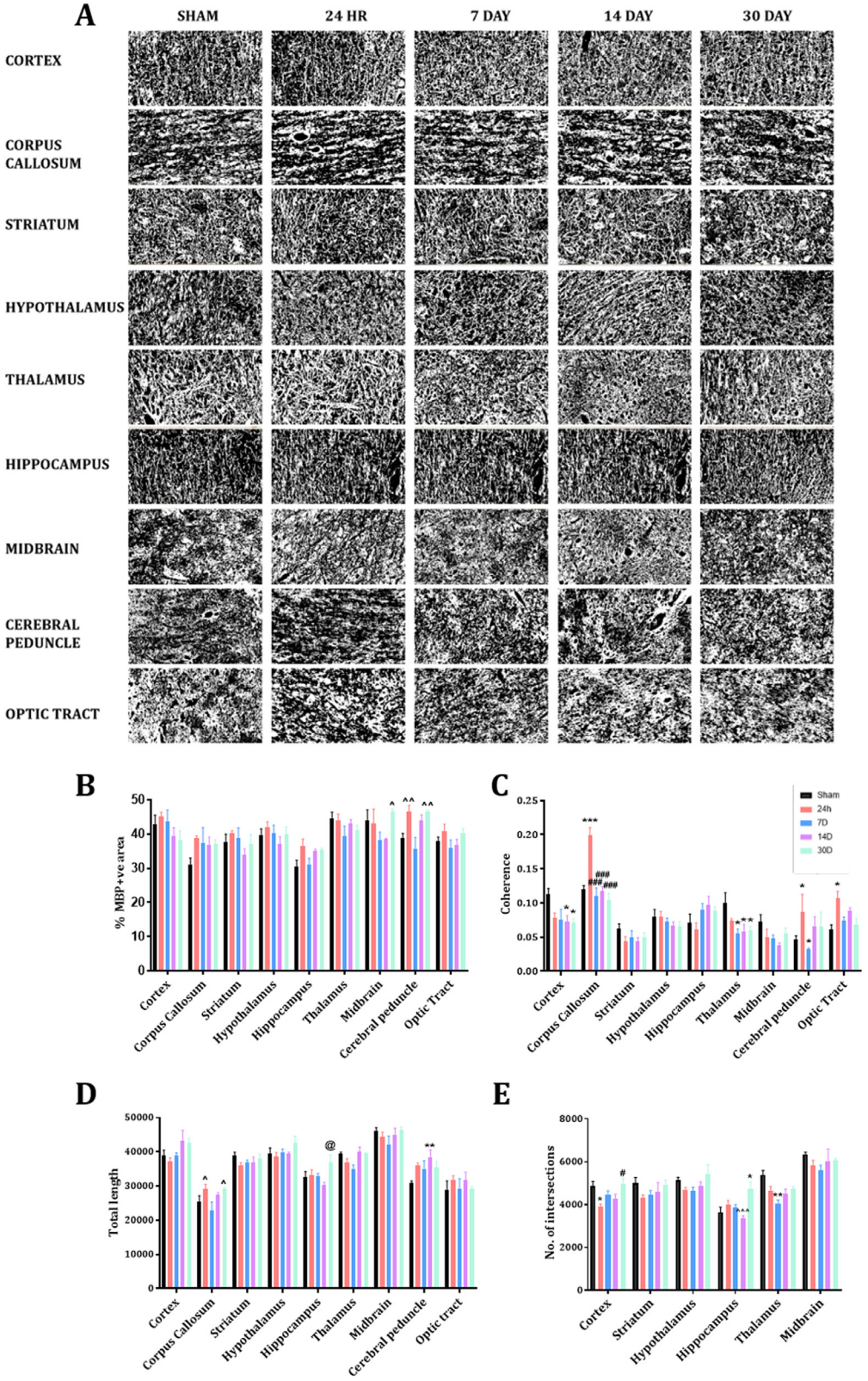

Fig. 7. Representative images of MBP immunohistochemistry from our regions of interest following removal of background, thresholding and creation of a binary image (A), with evaluation of the effects of TBI on expression of MBP as examined via% area stained (B), coherency (C), total myelin length (D) and number of intersections (E). Scale bar = 50 μm. Image representative of $n = 5$ per group. (* = $p<0.05$; ** = $p < 0.01$: *** = $p < 0.001$); # indicates significantly different compared to 24 h (# = $p<0.05$; ## = $p<0.01$; ### = $p<0.001$) ^$p<0.05$, ^^$p<0.01$ indicates significantly different compared to 7 D animals.

Table. 1
Summary of results of myelin analysis.

		Cerebral peduncle	Optic Tract	Corpus callosum	Mid-brain	Hippo-campus	Thalamus	Hypo-thalamus	Striatum	Cortex
24hrs	% area	–	–	–	–	–	–	–	–	–
	Myelin length	–	–	–	–	–	–	–	–	–
	No. intersections	NA	NA	NA	–	–	–	–	–	↓
	Coherence	↑	↑	↑↑↑	–	–	–	–	–	–
7 D	% area	–	–	–	–	–	–	–	–	–
	Myelin length	–	–	–	–	–	–	–	–	–
	No. intersections	NA	NA	NA	–	–	↓	–	–	–
	Coherence	–	–	–	–	–	↓		–	–
14 D	% area	–	–	–	–	–	–	–	–	–
	Myelin length	–	–	–	–	–	–	–	–	–
	No. intersections	NA	NA	NA	–	–	–	–	–	–
	Coherence	–	–	–	–	–	↓		–	↓
30 D	% area	–	–	–	–	–	–	–	–	–
	Myelin length	–	–	–	–	–	–	–	–	–
	No. intersections	NA	NA	NA	–	↑↑	–	–	–	–
	Coherence	–	–	–	–	–	↓	–	–	↓

- no change ↓ $p < 0.05$, ↑↑ $p < 0.01$, ↑↑↑ $p < 0.001$ compared to sham animals. NA = not applicable for this region.

by APP immunohistochemistry

Indeed, although no overall loss of MBP relative to sham animals was noted in any region or at any time-point post-injury, subtle changes in the microstructural organization of these fibres were noted within the grey matter in the cortex under the impact site, thalamus, and hippocampus. This is supported by DTI, with changes seen within the cortex, thalamus, and hippocampus, and volumetric changes within the thalamus and hippocampus. In the cortex, decreased MD values were seen at 7 D, 14 D, and 30 D post-injury caused by a decrease in RD at 14 D and AD at 24 h, 14 D, and 30 D via DTI. Previous studies have suggested that concomitant reductions in AD/RD within grey matter indicate hindered water diffusion, which may be linked to cytotoxic oedema (Takayama et al., 2000), increased neurite density (Blumenfeld-Katzir et al., 2011), or the presence of plaques or other diffusion hindering materials including glial cells (Baugh et al., 2012). Cytotoxic oedema results from the sustained intracellular water accumulation, mainly caused by active ion pump failure (e.g., Na+/K+-ATPase), resulting in cell swelling and decreased interstitial space (Liang et al., 2007). Clinically, predominant cortical cytotoxic oedema has been noted on MRI up to 7 D post-injury in half of TBI patients (Hudak et al., 2014). In rodent TBI models, the mixed lateral fluid percussion model found ipsilateral oedema began as early as 1 h post-injury, was maximal at 48 h, and resorbed by 7 D (Bareyre et al., 1997), with O'Connor et al. showing the presence of cortical oedema out to 5 D post-injury following diffuse injury (O'Connor et al., 2006), suggesting this may play a role in the impaired diffusion noted sub-acutely here. Furthermore, our own results suggest alterations in microstructure within the cortex with decreased coherence (reflecting increased complexity) and decreased number of intersections of MBP+ve fibres in the cortex. This may suggest that although neurite outgrowth is stimulated in the subacute phase post-injury, this is not sufficient to restore connectivity at the time-points examined. Indeed, levels of GAP-43, a protein associated with synaptic remodelling and neuronal sprouting, are increased within the cortex following mild-moderate TBI (Corrigan et al., 2012; Thompson et al., 2006), suggesting that this may be occurring in this model.

These DTI changes may also be the result of underlying neuroinflammation, as this pathology within the grey matter was supported via the examination of the number of activated microglia, as seen as a change in morphology, which found increases within the cortex, hypothalamus, hippocampus, midbrain, and thalamus, primarily peaking at 24 h post-injury. This phenomenon has been investigated in different animal models of TBI showing persistent and prolonged microglia activation weeks (Arulsamy et al., 2018; Donat et al., 2017; Elliott et al., 2011), months (Arulsamy et al., 2018; Glushakova et al., 2014; Holmin and Mathiesen, 1999), and even years (Loane et al., 2014) following TBI. TBI leads to the initiation of an inflammatory in response to cellular damage and an associated release of factors that act as damage-associated molecules (Corrigan et al., 2016). These bind to toll-like receptors on resident immune cells, like microglia, causing their activation and release of inflammatory mediators (Loane and Kumar, 2016). As the activation state here was assessed by appearance, with activated microglia becoming either hyper-ramified with an enlarged cell body or having an enlarged cell body with a reduction in process number (Evilsizor et al., 2015), we cannot differentiate between the phenotype to determine what role these microglia were playing post-injury. However previous studies suggest that there is an early peak in M2-like activated microglia in the week following injury (Jin et al., 2012; Wang et al., 2013), which then shifts to a maladaptive M1-like activation at later time points (Loane and Kumar, 2016). Thus, the continued presence of activated microglia within the thalamus at 30 D post-injury is suggestive of ongoing pathology within this area. This is supported by the increase in volume noted and changes in FA and RD values, as well as microstructural analysis of MBP+ve fibres showing decreased coherence from 7D–30D post-injury and fewer intersections at 7D post-injury. Indeed, imaging studies using [11C]PK11195 and [123I]CLINDE, as a marker of the translocator protein expressed by activated microglia, have shown increased binding associated with microglial activation within the thalamus in the sub-acute phase (30D post-injury) (Donat et al., 2017) and also chronically (17 years post-injury) (Ramlackhansingh et al., 2011), with this supported by immunohistochemical studies (Raghavendra Rao et al., 2000). This thalamic inflammation is linked to damage of cortico-thalamic projections, leading to retrograde microglial activation within the thalamus (Scott et al., 2015). Indeed, as the thalamus receives a high density of projection neurons from the cortex, it allows amplification of cortical pathology. Evidence of ongoing microglia activation, as seen here, highlights the vulnerability of the thalamus to secondary neurodegeneration post-TBI. This is important as alterations in thalamic DTI parameters (FA and mean kurtosis) are linked to poorer cognitive outcome (Grossman et al., 2012) and suggests that the thalamus may be a key brain region to monitor for temporal changes post-injury.

DTI also suggested the hippocampus as a key site affected by TBI, with a decrease in hippocampal volume, increased FA and decreased RD at 30 D post-injury. This is in line with clinical reports of reduced hippocampal volume chronically, up to two years post-injury, following moderate-to-severe head injury (Ariza et al., 2006). Previous studies have shown a relationship between DTI measurements and neuroinflammatory changes post-TBI (Budde et al., 2011). For example, Yu and colleagues showed that decreased AD values within the cortex correlated strongly with increases in microglial reactivity (Yu et al., 2017). Robinson and colleagues similarly found that decreases in AD within

both grey and white matter structures was associated with microglial proliferation and activation (Robinson et al., 2017), in line with the findings here. It should be noted that this relationship is complex; for example, in white matter, astrocytic reactivity in response to axonal damage was associated with decreases in FA in the chronic period, but not the acute period (MacDonald et al., 2007), suggesting that it is the cumulative effects of injury encompassing factors such as neuroinflammation, axonal damage, and swelling amongst others that alter DTI parameters, which cannot be attributed to a single source. Nonetheless, we have shown here that sites that show evidence of persistent neuroinflammation and microstructural alterations post-TBI histologically, similarly show alterations on DTI, suggesting a link between the two. Indeed, histological evaluation found persistent activation of microglia noted to 30 D post-injury. Microstructural alterations were also noted with an increase in the number of MBP + ve intersections at 30 D post-injury, in line with reports of synaptogenesis within the CA1 region of the hippocampus from day 10 following a focal injury (Scheff et al., 2005).

Although this study did not directly assess behaviour, we have previously reported that at one-month post-injury, animals showed no cognitive deficits on the Y Maze, anxiety deficits on the Elevated Plus Maze, or locomotor deficits on the rotarod, but did have increased depressive-like behaviour on the forced swim test (Arulsamy et al., 2018). Indeed, even at 12 months post-injury, only subtle executive function deficits were noted post-TBI, although the methods used were inadequate to determine whether depressive-like behaviour was present (Arulsamy et al., 2019). However, it is well known that a history of TBI is linked to increased risk of later dementia (Fann et al., 2018; Kenney and Diaz-Arrastia, 2018), associated with persistent chronic neuroinflammation and consequent neurodegeneration (Loane et al., 2014). Given the persistent DTI changes seen here and the links with ongoing neuroinflammation, especially within the thalamus and hippocampus, pathology within these areas may be driving the link between TBI and later neurodegeneration, with future studies needed to investigate this.

Future studies could also extend these DTI findings by using more sophisticated diffusion imaging techniques, such as neurite orientation dispersion and density imaging (NODDI), which models water diffusion in distinct compartments (inter-neurite vs extra-neurite). In particular, the neurite density index (NDI) based on the intracellular volume fraction to reflect axonal density (Zhang et al., 2012) has been found to decrease over time following mild TBI clinically within white matter tracts (Palacios et al., 2018). Apparent fibre density (AFD) is another alternative metric which assesses the fraction of space occupied by a fibre bundle and is based on analysis of fibre orientation distribution, and thus, reduces the effects of crossing fibres as a confound, as occurs in DTI analysis (Raffelt et al., 2017). Indeed, decreases in AFD have been noted at 12 months post-LFP injury within widespread white matter tracts (Wright et al., 2017a). Importantly, both AFD and NODDI have been shown to be more sensitive than traditional DTI metrics in detecting microstructural changes following TBI (Wright et al., 2017a), thereby suggesting a shift towards newer neuroimaging methodologies is required.

It should be noted that, as this study was designed for longitudinal assessment of alterations in DTI parameters, different cohorts of animals were used for immunohistochemical analyses. Thus, we cannot directly correlate between the imaging and the immunohistochemistry data. Furthermore, another major limitation was the lack of sham animals within the imaging cohort, and thus the changes described here could potentially be caused by the effects of anaesthesia or age. It should be noted that previous studies utilizing a similar time-course and repeat imaging did not see changes in DTI parameters in their shams (Braeckman et al., 2019; Hoogenboom et al., 2019), but this would need to be confirmed in our cohort. Furthermore, the pooling of shams from both acute and chronic time-points for the histological analysis could similarly confound results, as the peripheral insult could induce neuroinflammation acutely. In our previous studies, we have not noted significant effects in acute versus chronic shams in regards to the degree of microglial activation (Collins-Praino et al., 2018), but this factor cannot be ruled out. Furthermore, this study only included male animals, with increasing literature highlighting that sex influences the response to TBI (Berry et al., 2009; Munivenkatappa et al., 2016; Phelan et al., 2007; Roof and Hall, 2000). In particular, the inflammatory response to TBI appears to differ depending on sex, with pre-clinical TBI research finding that male mice have faster and more pronounced microglial activation than female mice post-CCI injury (Villapol et al., 2017). This may account for reports of greater white matter damage in males compared to females following mild TBI and repeated mild TBI (Fakhran et al., 2014; Wright et al., 2017b). Of note, females showed more damage to the grey matter of the PFC (Wright et al., 2017b) post-repeated mild TBI, suggesting that a comprehensive comparison of the spatiotemporal effects of TBI on neuroinflammation and subsequent microstructural damage are required.

5. Conclusion

This work provides an overview of the spatiotemporal profile of the microstructural changes induced following a TBI exploiting both DTI and histological measures. Alongside the extensive white matter alterations noted, diffuse TBI had widespread and persistent effects on grey matter including the cortex, hippocampus, and thalamus. This provides an anatomical overview for understanding the basis of persistent alterations in cognition and mood following TBI and highlights the need to examine recovery not only within white matter tracts but in associated grey matter regions.

CRediT authorship contribution statement

Abdalla Z Mohamed: Data curation, Writing - review & editing. **Frances Corrigan:** Data curation, Writing - review & editing. **Lyndsey E. Collins-Praino:** Data curation. **Stephanie L. Plummer:** Data curation. **Neha Soni:** Data curation. **Fatima A. Nasrallah:** Writing - review & editing.

Declaration of Competing Interest

The authors report no competing interests.

Acknowledgement and funding

This work as supported by Motor Accident Insurance Commission (MAIC) (Grant:2014000857), the Queensland Government, Australia for the research grant to FN. This work was also supported by grants from the Neurosurgical Research Foundation to FC and LCP. We thank the Australian Government support through NCRIS and the National Imaging Facility for the operation of 9.4T MRI at Centre of Advanced Imaging, University of Queensland, Brisbane, Australia. We thank Jessica Sharkey and Michail Laoumtzis for technical assistance.

Supplementary materials

Supplementary material associated with this article can be found, in the online version, at doi:10.1016/j.nicl.2019.102136.

References

Arfanakis, K., Haughton, V.M., Carew, J.D., Rogers, B.P., Dempsey, R.J., Meyerand, M.E., 2002. Diffusion tensor MR imaging in diffuse axonal injury. AJNR Am. J. Neuroradiol. 23, 794–802.

Ariza, M., Serra-Grabulosa, J.M., Junqué, C., Ramírez, B., Mataró, M., Poca, A., Bargalló, N., Sahuquillo, J., 2006. Hippocampal head atrophy after traumatic brain injury. Neuropsychologia 44, 1956–1961. https://doi.org/10.1016/j.neuropsychologia.2005.11.007.

Armstrong, R.C., Mierzwa, A.J., Marion, C.M., Sullivan, G.M., 2016. White matter

involvement after TBI: clues to axon and myelin repair capacity. Exp. Neurol. 275, 328–333. https://doi.org/10.1016/j.expneurol.2015.02.011.
Arulsamy, A., Teng, J., Colton, H., Corrigan, F., Collins-Praino, L., 2018. Evaluation of early chronic functional outcomes and their relationship to pre-frontal cortex and hippocampal pathology following moderate-severe traumatic brain injury. Behav. Brain Res. 348, 127–138. https://doi.org/10.1016/j.bbr.2018.04.009.
Bareyre, F., Wahl, F., McIntosh, T.K., Stutzmann, J.M., 1997. Time course of cerebral edema after traumatic brain injury in rats: effects of riluzole and mannitol. J. Neurotrauma 14, 839–849.
Baugh, C.M., Stamm, J.M., Riley, D.O., Gavett, B.E., Shenton, M.E., Lin, A., Nowinski, C.J., Cantu, R.C., McKee, A.C., Stern, R.A., 2012. Chronic traumatic encephalopathy: neurodegeneration following repetitive concussive and subconcussive brain trauma. Brain Imaging Behav 6, 244–254. https://doi.org/10.1007/s11682-012-9164-5.
Bazarian, J.J., Zhong, J., Blyth, B., Zhu, T., Kavcic, V., Peterson, D., 2007. Diffusion tensor imaging detects clinically important axonal damage after mild traumatic brain injury: a pilot study. J. Neurotrauma 24, 1447–1459. https://doi.org/10.1089/neu.2007.0241.
Behrens, T.E.J., Woolrich, M.W., Jenkinson, M., Johansen-Berg, H., Nunes, R.G., Clare, S., Matthews, P.M., Brady, J.M., Smith, S.M., 2003. Characterization and propagation of uncertainty in diffusion-weighted MR imaging. Magn. Reson. Med. 50, 1077–1088. https://doi.org/10.1002/mrm.10609.
Berry, C., Ley, E.J., Tillou, A., Cryer, G., Margulies, D.R., Salim, A., 2009. The effect of gender on patients with moderate to severe head injuries. J. Trauma – Inj. Infect. Crit. Care 67, 950–953. https://doi.org/10.1097/TA.0b013e3181ba3354.
Blennow, K., Brody, D.L., Kochanek, P.M., Levin, H., McKee, A., Ribbers, G.M., Yaffe, K., Zetterberg, H., 2016. Traumatic brain injuries. Nat. Rev. Dis. Prim. 2, 16084. https://doi.org/10.1038/nrdp.2016.84.
Blumenfeld-Katzir, T., Pasternak, O., Dagan, M., Assaf, Y., 2011. Diffusion MRI of structural brain plasticity induced by a learning and memory task. PLoS ONE 6, e20678. https://doi.org/10.1371/journal.pone.0020678.
Bouix, S., Pasternak, O., Rathi, Y., Pelavin, P.E., Zafonte, R., Shenton, M.E., 2013. Increased gray matter diffusion anisotropy in patients with persistent post-concussive symptoms following mild traumatic brain injury. PLoS ONE 8, e66205. https://doi.org/10.1371/journal.pone.0066205.
Braeckman, K., Descamps, B., Pieters, L., Vral, A., Caeyenberghs, K., Vanhove, C., 2019. Dynamic changes in hippocampal diffusion and kurtosis metrics following experimental mTBI correlate with glial reactivity. NeuroImage Clin. 21, 101669. https://doi.org/10.1016/J.NICL.2019.101669.
Bramlett, H.M., Dietrich, W.D., 2004. Pathophysiology of cerebral ischemia and brain trauma: similarities and differences. J. Cereb. Blood Flow Metab. 24, 133–150. https://doi.org/10.1097/01.WCB.0000111614.19196.04.
Budde, M.D., Janes, L., Gold, E., Turtzo, L.C., Frank, J.A., 2011. The contribution of gliosis to diffusion tensor anisotropy and tractography following traumatic brain injury: validation in the rat using Fourier analysis of stained tissue sections. Brain 134, 2248–2260. https://doi.org/10.1093/brain/awr161.
Chang, E.H., Argyelan, M., Chandon, T.S.S., Karlsgodt, K.H., Mori, S., Malhotra, A.K., 2017. Diffusion tensor imaging measures of white matter compared to myelin basic protein immunofluorescence in tissue cleared intact brains. Data Br. 10, 438–443. https://doi.org/10.1016/j.dib.2016.12.018.
Chou, N., Wu, J., Bai Bingren, J., Qiu, A., Chuang, K.-.H., 2011. Robust automatic rodent brain extraction using 3-D pulse-coupled neural networks (PCNN). IEEE Trans. Image Process 20, 2554–2564. https://doi.org/10.1109/TIP.2011.2126587.
Collins-Praino, L.E., Arulsamy, A., Katharesan, V., Corrigan, F., 2018. The effect of an acute systemic inflammatory insult on the chronic effects of a single mild traumatic brain injury. Behav. Brain Res. 336, 22–31. https://doi.org/10.1016/j.bbr.2017.08.035.
Corrigan, F., Vink, R., Blumbergs, P.C., Masters, C.L., Cappai, R., Van Den Heuvel, C., 2012. Characterisation of the effect of knockout of the amyloid precursor protein on outcome following mild traumatic brain injury. Brain Res. 1451, 87–99. https://doi.org/10.1016/j.brainres.2012.02.045.
Corrigan, F., Vink, R., Turner, R.J., 2016. Inflammation in acute CNS injury: a focus on the role of substance P. Br. J. Pharmacol. 173, 703–715. https://doi.org/10.1111/bph.13155.
Corrigan, F., Ziebell, J.M., Vink, R., 2011. Models of rodent cortical traumatic brain injury. Neuromethods 62, 193–209. https://doi.org/10.1007/978-1-61779-301-1_11.
Dikranian, K., Cohen, R., Mac Donald, C., Pan, Y., Brakefield, D., Bayly, P., Parsadanian, A., 2008. Mild traumatic brain injury to the infant mouse causes robust white matter axonal degeneration which precedes apoptotic death of cortical and thalamic neurons. Exp. Neurol. 211, 551–560. https://doi.org/10.1016/j.expneurol.2008.03.012.
DiLeonardi, A.M., Huh, J.W., Raghupathi, R., 2009. Impaired axonal transport and neurofilament compaction occur in separate populations of injured axons following diffuse brain injury in the immature rat. Brain Res. 1263, 174–182. https://doi.org/10.1016/j.brainres.2009.01.021.
Donat, C.K., Scott, G., Gentleman, S.M., Sastre, M., 2017. Microglial activation in traumatic brain injury. Front. Aging Neurosci. 9, 208. https://doi.org/10.3389/fnagi.2017.00208.
Elliott, M.B., Tuma, R.F., Amenta, P.S., Barbe, M.F., Jallo, J.I., 2011. Acute effects of a selective cannabinoid-2 receptor agonist on neuroinflammation in a model of traumatic brain injury. J. Neurotrauma 28, 973–981. https://doi.org/10.1089/neu.2010.1672.
Evilsizor, M.N., Ray-Jones, H.F., Ellis, T.W., Lifshitz, J., Ziebell, J.M., 2015. Microglia in experimental brain injury: implications on neuronal injury and circuit remodeling. In: Kobeissy, FH (Ed.), Brain Neurotrauma: Molecular, Neuropsychological, and Rehabilitation Aspects. CRC Press/Taylor & Francis, Boca Raton (FL). https://doi.org/10.1201/b18126. https://www.ncbi.nlm.nih.gov/books/NBK299191/.
Fakhran, S., Yaeger, K., Collins, M., Alhilali, L., 2014. Sex differences in white matter abnormalities after mild traumatic brain injury: localization and correlation with outcome. Radiology 272, 815–823. https://doi.org/10.1148/radiol.14132512.
Fann, J.R., Ribe, A.R., Pedersen, H.S., Fenger-Grøn, M., Christensen, J., et al., 2018. Long-term risk of dementia among people with traumatic brain injury in Denmark: a population-based observational cohort study. The Lancet Psychiatry 5, 424–431. https://doi.org/10.1016/S2215-0366(18)30065-8.
Finfer, S., Cohen, J., 2001. Severe traumatic brain injury. Resuscitation 48, 77–90.
Foda, M., Marmarou, A., 1994. A new model of diffuse brain injury in rats. Part II: morphological characterization. J. Neurosurg. 80, 301–313. https://doi.org/10.3171/jns.1994.80.2.0301.
Gale, S.D., Johnson, S.C., Bigler, E.D., Blatter, D.D., 1995. Nonspecific white matter degeneration following traumatic brain injury. J. Int. Neuropsychol. Soc. 1, 17–28. https://doi.org/10.1017/S1355617700000060.
Glushakova, O.Y., Johnson, D., Hayes, R.L., 2014. Delayed increases in microvascular pathology after experimental traumatic brain injury are associated with prolonged inflammation, blood-brain barrier disruption, and progressive white matter damage. J. Neurotrauma 31, 1180–1193. https://doi.org/10.1089/neu.2013.3080.
Grossman, E.J., Ge, Y., Jensen, J.H., Babb, J.S., Miles, L., Reaume, J., Silver, J.M., Grossman, R.I., Inglese, M., 2012. Thalamus and cognitive impairment in mild traumatic brain injury: a diffusional kurtosis imaging study. J. Neurotrauma 29, 2318–2327. https://doi.org/10.1089/neu.2011.1763.
Hellewell, S.C., Yan, E.B., Agyapomaa, D.A., Bye, N., Morganti-Kossmann, M.C., 2010. Post-traumatic hypoxia exacerbates brain tissue damage: analysis of axonal injury and glial responses. J. Neurotrauma 27, 1997–2010. https://doi.org/10.1089/neu.2009.1245.
Holmin, S., Mathiesen, T., 1999. Long-term intracerebral inflammatory response after experimental focal brain injury in rat. Neuroreport 10, 1889–1891. https://doi.org/10.1097/00001756-199906230-00017.
Hoogenboom, W.S., Rubin, T.G., Ye, K., Cui, M.-.H., Branch, K.C., Liu, J., Branch, C.A., Lipton, M.L., 2019. Diffusion tensor imaging of the evolving response to mild traumatic brain injury in rats. J. Exp. Neurosci. 13, 1179069519858627. https://doi.org/10.1177/1179069519858627.
Hudak, A.M., Peng, L., De La Plata, C.M., Thottakara, J., Moore, C., Harper, C., Mccoll, R., Babcock, E., Diaz-Arrastia, R., 2014. Cytotoxic and vasogenic cerebral oedema in traumatic brain injury: assessment with flair and DWI imaging. Brain Inj. 28, 1602–1609. https://doi.org/10.3109/02699052.2014.936039.
Hulkower, M.B., Poliak, D.B., Rosenbaum, S.B., Zimmerman, M.E., Lipton, M.L., 2013. A decade of DTI in traumatic brain injury: 10 years and 100 articles later. Am. J. Neuroradiol. 34, 2064–2074. https://doi.org/10.3174/ajnr.A3395.
Inglese, M., Makani, S., Johnson, G., Cohen, B.a., Silver, J.a., Gonen, O., Grossman, R.I., 2005. Diffuse axonal injury in mild traumatic brain injury: a diffusion tensor imaging study. J. Neurosurg. 103, 298–303. https://doi.org/10.3171/jns.2005.103.2.0298.
Jenkinson, M., Bannister, P., Brady, M., Smith, S., 2002. Improved optimization for the robust and accurate linear registration and motion correction of brain images. Neuroimage 17, 825–841. https://doi.org/10.1016/S1053-8119(02)91132-8.
Jin, X., Ishii, H., Bai, Z., Itokazu, T., Yamashita, T., 2012. Temporal changes in cell marker expression and cellular infiltration in a controlled cortical impact model in adult male C57BL/6 mice. PLoS ONE 7, e41892. https://doi.org/10.1371/journal.pone.0041892.
Johnson, V.E., Stewart, W., Smith, D.H., 2013. Axonal pathology in traumatic brain injury. Exp. Neurol. 246, 35–43. https://doi.org/10.1016/j.expneurol.2012.01.013.
Johnstone, V.P.A., Wright, D.K., Wong, K., O'Brien, T.J., Rajan, R., Shultz, S.R., 2015. Experimental traumatic brain injury results in long-term recovery of functional responsiveness in sensory cortex but persisting structural changes and sensorimotor, cognitive, and emotional deficits. J. Neurotrauma 32, 1333–1346. https://doi.org/10.1089/neu.2014.3785.
Kenney, K., Diaz-Arrastia, R., 2018. Risk of dementia outcomes associated with traumatic brain injury during military service. JAMA Neurol 75, 1043–1044. https://doi.org/10.1001/jamaneurol.2018.034.
Lepage, C., de Pierrefeu, A., Koerte, I.K., Coleman, M.J., Pasternak, O., Grant, G., Marx, C.E., Morey, R.A., Flashman, L.A., George, M.S., McAllister, T.W., Andaluz, N., Shutter, L., Coimbra, R., Zafonte, R.D., Stein, M.B., Shenton, M.E., Bouix, S., 2017. White matter abnormalities in mild traumatic brain injury with and without post-traumatic stress disorder: a subject-specific diffusion tensor imaging study. Brain Imaging Behav 12, 870–881. https://doi.org/10.1007/s11682-017-9744-5.
Li, J., Li, X.-.Y., Feng, D.-.F., Gu, L., 2011. Quantitative evaluation of microscopic injury with diffusion tensor imaging in a rat model of diffuse axonal injury. Eur. J. Neurosci. 33, 933–945. https://doi.org/10.1111/j.1460-9568.2010.07573.x.
Liang, D., Bhatta, S., Gerzanich, V., Simard, J.M., 2007. Cytotoxic edema: mechanisms of pathological cell swelling. Neurosurg. Focus 22, E2.
Ling, J.M., Peña, A., Yeo, R.A., Merideth, F.L., Klimaj, S., Gasparovic, C., Mayer, A.R., 2012. Biomarkers of increased diffusion anisotropy in semi-acute mild traumatic brain injury: a longitudinal perspective. Brain 135, 1281–1292. https://doi.org/10.1093/brain/aws073.
Loane, D.J., Kumar, A., 2016. Microglia in the TBI brain: the good, the bad, and the dysregulated. Exp. Neurol. 275, 316–327. https://doi.org/10.1016/j.expneurol.2015.08.018.
Loane, D.J., Kumar, A., Stoica, B.A., Cabatbat, R., Faden, A.I., 2014. Progressive neurodegeneration after experimental brain trauma: association with chronic microglial activation. J. Neuropathol. Exp. Neurol. 73, 14–29. https://doi.org/10.1097/NEN.0000000000000021.
Maas, A., 2016. Traumatic brain injury: changing concepts and approaches. Chinese J. Traumatol. 19, 3–6. https://doi.org/10.1016/j.cjtee.2016.01.001.
Maas, A.I., Stocchetti, N., Bullock, R., 2008. Moderate and severe traumatic brain injury in adults. Lancet Neurol 7, 728–741. https://doi.org/10.1016/S1474-4422(08)70164-9.

Donald, Mac, C.L., Dikranian, K., Song, S.K., Bayly, V., P., Holtzman, D.M., Brody, D.L., 2007. Detection of traumatic axonal injury with diffusion tensor imaging in a mouse model of traumatic brain injury. Exp. Neurol. 205, 116–131. https://doi.org/10.1016/j.expneurol.2007.01.035.

MacDonald, C.L., Dikranian, K., Bayly, P., Holtzman, D., Brody, D., 2007. Diffusion tensor imaging reliably detects experimental traumatic axonal injury and indicates approximate time of injury. J. Neurosci. 27, 11869–11876. https://doi.org/10.1523/JNEUROSCI.3647-07.2007.

Marmarou, A., Foda, M., van den Brink, W., Campbell, J., Kita, H., Demetriadou, K., 1994. A new model of diffuse brain injury in rats. Part I: Pathophysiol. Biomech. J. Neurosurg. 80, 291–300. https://doi.org/10.3171/jns.1994.80.2.0291.

Matsushita, M., Hosoda, K., Naitoh, Y., Yamashita, H., Kohmura, E., 2011. Utility of diffusion tensor imaging in the acute stage of mild to moderate traumatic brain injury for detecting white matter lesions and predicting long-term cognitive function in adults: clinical article. J. Neurosurg. 115, 130–139. https://doi.org/10.3171/2011.2.JNS101547.

Mayer, A.R., Ling, J., Mannell, M.V., Gasparovic, C., Phillips, J.P., Doezema, D., Reichard, R., Yeo, R.A., 2010. A prospective diffusion tensor imaging study in mild traumatic brain injury. Neurology 74, 643–650. https://doi.org/10.1212/WNL.0b013e3181d0ccdd.

Ming, C.L., Akle, V., Zheng, W., Kitlen, J., O'Steen, B., Larner, S.F., Dave, J.R., Tortella, F.C., Hayes, R.L., Wang, K.K.W., 2006. Extensive degradation of myelin basic protein isoforms by calpain following traumatic brain injury. J. Neurochem. 98, 700–712. https://doi.org/10.1111/j.1471-4159.2006.03882.x.

Mohamed, A.Z., Cumming, P., Götz, J., Nasrallah, F., for the Department of Defense Alzheimer's Disease Neuroimaging Initiative, 2019. Tauopathy in veterans with long-term posttraumatic stress disorder and traumatic brain injury. Eur. J. Nucl. Med. Mol. Imaging 46, 1139–1151. https://doi.org/10.1007/s00259-018-4241-7.

Mohamed, A.Z., Cumming, P., Srour, H., Gunasena, T., Uchida, A., Haller, C.N., the Department of Defense Alzheimer's Disease Neuroimaging Initiative, 2018. Amyloid pathology fingerprint differentiates post-traumatic stress disorder and traumatic brain injury. NeuroImage Clinical 19, 716–726. https://doi.org/10.1016/J.NICL.2018.05.016.

Munivenkatappa, A., Agrawal, A., Shukla, D.P., Kumaraswamy, D., Devi, B.I., 2016. Traumatic brain injury: does gender influence outcomes? Int. J. Crit. Illn. Inj. Sci 6, 70–73. https://doi.org/10.4103/2229-5151.183024.

O'Connor, C.A., Cernak, I., Vink, R., 2006. The temporal profile of edema formation differs between male and female rats following diffuse traumatic brain injury. Acta Neurochir. Suppl. 96, 121–124. https://doi.org/10.1007/3-211-30714-1_27.

Otsuka, N., Tomonaga, M., Ikeda, K., 1991. Rapid appearance of β-amyloid precursor protein immunoreactivity in damaged axons and reactive glial cells in rat brain following needle stab injury. Brain Res. 568, 335–338. https://doi.org/10.1016/0006-8993(91)91422-W.

Palacios, E., Owen, J.P., Yuh, E.L., Wang, M.B., Vassar, M.J., Ferguson, A.R., Diaz-Arrastia, R., Giacino, J.T., Okonkwo, D.O., Robertson, C.S., Stein, M.B., Temkin, N., Jain, S., McCrea, M., Donald, C.L.M., Manley, G.T., Mukherjee, P., Investigators, T.-T., 2018. The evolution of white matter microstructural changes after mild traumatic brain injury: a longitudinal DTI and Noddi study. bioRxiv. https://doi.org/10.1101/345629.

Peled, S., 2007. New perspectives on the sources of white matter DTI signal. IEEE Trans. Med. Imaging 26, 1448–1455. https://doi.org/10.1109/TMI.2007.906787.

Phelan, H.A., Shafi, S., Parks, J., Maxson, R.T., Ahmad, N., Murphy, J.T., Minei, J.P., 2007. Use of a pediatric cohort to examine gender and sex hormone influences on outcome after trauma. J. Trauma – Inj. Infect. Crit. Care 63, 1127–1131. https://doi.org/10.1097/TA.0b013e318154c1b8.

Pierpaoli, C., Basser, P.J., 1996. Toward a quantitative assessment of diffusion anisotropy. Magn. Reson. Med. 36, 893–906. https://doi.org/10.1002/mrm.1910360612.

Plummer, S.L., Corrigan, F., Thornton, E., Woenig, J.A., Vink, R., Cappai, R., Heuvel, D., Van, C., 2018. The amyloid precursor protein derivative, APP96-110, is efficacious following intravenous administration after traumatic brain injury. PLoS ONE 13, e0190449. https://doi.org/10.1371/journal.pone.0190449.

Raffelt, D.A., Tournier, J.D., Smith, R.E., Vaughan, D.N., Jackson, G., Ridgway, G.R., Connelly, A., 2017. Investigating white matter fibre density and morphology using fixel-based analysis. Neuroimage 144, 58–73. https://doi.org/10.1016/j.neuroimage.2016.09.029.

Raghavendra Rao, V.L, Dogan, A., Bowen, K.K., Dempsey, R.J., 2000. Traumatic brain injury leads to increased expression of peripheral-type benzodiazepine receptors, neuronal death, and activation of astrocytes and microglia in rat thalamus. Exp. Neurol. 161, 102–114. https://doi.org/10.1006/exnr.1999.7269.

Ramlackhansingh, A.F., Brooks, D.J., Greenwood, R.J., Bose, S.K., Turkheimer, F.E., Kinnunen, K.M., Gentleman, S., Heckemann, R.A., Gunanayagam, K., Gelosa, G., Sharp, D.J., 2011. Inflammation after trauma: microglial activation and traumatic brain injury. Ann. Neurol. 70, 374–383. https://doi.org/10.1002/ana.22455.

Robinson, S., Berglass, J.B., Denson, J.L., Berkner, J., Anstine, C.V., Winer, J.L., Maxwell, J.R., Qiu, J., Yang, Y., Sillerud, L.O., Meehan, W.P., Mannix, R., Jantzie, L.L., 2017. Microstructural and microglial changes after repetitive mild traumatic brain injury in mice. J. Neurosci. Res. 95, 1025–1035. https://doi.org/10.1002/jnr.23848.

Roof, R.L., Hall, E.D., 2000. Gender differences in acute CNS trauma and stroke: neuroprotective effects of estrogen and progesterone. J. Neurotrauma 17, 367–388. https://doi.org/10.1089/neu.2000.17.367.

Rosenblum, W.I., 2007. Cytotoxic edema: monitoring its magnitude and contribution to brain swelling. J. Neuropathol. Exp. Neurol. 66, 771–778. https://doi.org/10.1097/nen.0b013e3181461965.

Rubin, T.G., Catenaccio, E., Fleysher, R., Hunter, L.E., Lubin, N., Stewart, W.F., Kim, M., Lipton, R.B., Lipton, M.L., 2018. MRI-defined white matter microstructural alteration associated with soccer heading is more extensive in women than men. Radiology 289, 478–486. https://doi.org/10.1148/radiol.2018180217.

Scheff, S.W., Price, D.A., Hicks, R.R., Baldwin, S.A., Robinson, S., Brackney, C., 2005. Synaptogenesis in the hippocampal CA1 field following traumatic brain injury. J. Neurotrauma 22, 719–732. https://doi.org/10.1089/neu.2005.22.719.

Scholz, J., Tomassini, V., Johansen-Berg, H., 2014. Individual Differences in White Matter Microstructure in the Healthy Brain, in: Diffusion MRI. Elsevier, pp. 301–316. https://doi.org/10.1016/B978-0-12-396460-1.00014-7.

Schwarz, A.J., Danckaert, A., Reese, T., Gozzi, A., Paxinos, G., Watson, C., Merlo-Pich, E.V., Bifone, A., 2006. A stereotaxic mri template set for the rat brain with tissue class distribution maps and co-registered anatomical atlas: application to pharmacological MRI. Neuroimage 32, 538–550. https://doi.org/10.1016/j.neuroimage.2006.04.214.

Scott, G., Hellyer, P.J., Ramlackhansingh, A.F., Brooks, D.J., Matthews, P.M., Sharp, D.J., 2015. Thalamic inflammation after brain trauma is associated with thalamo-cortical white matter damage. J. Neuroinflammation 12, 244. https://doi.org/10.1186/s12974-015-0445-y.

Shah, S., Yallampalli, R., Merkley, T.L., McCauley, S.R., Bigler, E.D., MacLeod, M., Chu, Z., Li, X., Troyanskaya, M., Hunter, J.V., Levin, H.S., Wilde, E.A., 2012. Diffusion tensor imaging and volumetric analysis of the ventral striatum in adults with traumatic brain injury. Brain Inj. 26, 201–210. https://doi.org/10.3109/02699052.2012.654591.

Siedler, D.G., Chuah, M.I., Kirkcaldie, M.T.K., Vickers, J.C., King, A.E., 2014. Diffuse axonal injury in brain trauma: insights from alterations in neurofilaments. Front. Cell. Neurosci. 8, 429. https://doi.org/10.3389/fncel.2014.00429.

Singh, K., Trivedi, R., Devi, M.M., Tripathi, R.P., Khushu, S., 2016. Longitudinal changes in the DTI measures, anti-GFAP expression and levels of serum inflammatory cytokines following mild traumatic brain injury. Exp. Neurol. 275, 427–435. https://doi.org/10.1016/j.expneurol.2015.07.016.

Smith, D.H., Uryu, K., Saatman, K.E., Trojanowski, J.Q., McIntosh, T.K., 2003. Protein accumulation in traumatic brain injury. NeuroMolecular Med. 4, 59–72. https://doi.org/10.1385/NMM:4:1-2:59.

Sotak, C.H., 2002. The role of diffusion tensor imaging in the evaluation of ischemic brain – A review. NMR Biomed. 15, 561–569. https://doi.org/10.1002/nbm.786.

Taib, T., Leconte, C., Van Steenwinckel, J., Cho, A.H., Palmier, B., Torsello, E., Kuen, R.L., Onyeomah, S., Ecomard, K., Benedetto, C., Coqueran, B., Novak, A.C., Deou, E., Plotkine, M., Gressens, P., Marchand-Leroux, C., Besson, V.C., 2017. Neuroinflammation, myelin and behavior: temporal patterns following mild traumatic brain injury in mice. PLoS ONE 12, e0184811. https://doi.org/10.1371/journal.pone.0184811.

Takayama, H., Kobayashi, M., Sugishita, M., Mihara, B., 2000. Diffusion-weighted imaging demonstrates transient cytotoxic edema involving the corpus callosum in a patient with diffuse brain injury. Clin. Neurol. Neurosurg. 102, 135–139.

Thompson, S.N., Gibson, T.R., Thompson, B.M., Deng, Y., Hall, E.D., 2006. Relationship of calpain-mediated proteolysis to the expression of axonal and synaptic plasticity markers following traumatic brain injury in mice. Exp. Neurol. 201, 253–265. https://doi.org/10.1016/j.expneurol.2006.04.013.

Tournier, J.D., Mori, S., Leemans, A., 2011. Diffusion tensor imaging and beyond. Magn. Reson. Med. 65, 1532–1565. https://doi.org/10.1002/mrm.22924.

Tu, T.-W., Williams, R.A., Lescher, J.D., Jikaria, N., Turtzo, L.C., Frank, J.A., 2016. Radiological-pathological correlation of diffusion tensor and magnetization transfer imaging in a closed head traumatic brain injury model. Ann. Neurol. 79, 907–920. https://doi.org/10.1002/ana.24641.

van de Looij, Y., Mauconduit, F., Beaumont, M., Valable, S., Farion, R., Francony, G., Payen, J.F., Lahrech, H., 2012. Diffusion tensor imaging of diffuse axonal injury in a rat brain trauma model. NMR Biomed. 25, 93–103. https://doi.org/10.1002/nbm.1721.

Van Tilborg, E., Van Kammen, C.M., De Theije, C.G.M., Van Meer, M.P.A., Dijkhuizen, R.M., Nijboer, C.H., 2017. A quantitative method for microstructural analysis of myelinated axons in the injured rodent brain. Sci. Rep. 7, 16492. https://doi.org/10.1038/s41598-017-16797-1.

Villapol, S., Loane, D.J., Burns, M.P., 2017. Sexual dimorphism in the inflammatory response to traumatic brain injury. Glia 65, 1423–1438. https://doi.org/10.1002/glia.23171.

Wallace, E.J., Mathias, J.L., Ward, L., 2018. Diffusion tensor imaging changes following mild, moderate and severe adult traumatic brain injury: a meta-analysis. Brain Imaging Behav 12, 1607–1621. https://doi.org/10.1007/s11682-018-9823-2.

Wang, G., Zhang, J., Hu, X., Zhang, L., Mao, L., Jiang, X., Liou, A.K.-F., Leak, R.K., Gao, Y., Chen, J., 2013. Microglia/macrophage polarization dynamics in white matter after traumatic brain injury. J. Cereb. Blood Flow Metab. 33, 1864–1874. https://doi.org/10.1038/jcbfm.2013.146.

Ware, J.B., Hart, T., Whyte, J., Rabinowitz, A., Detre, J.A., Kim, J., 2017. Inter-Subject variability of axonal injury in diffuse traumatic brain injury. J. Neurotrauma 34, 2243–2253. https://doi.org/10.1089/neu.2016.4817.

Witcher, K.G., Eiferman, D.S., Godbout, J.P., 2015. Priming the inflammatory pump of the CNS after traumatic brain injury. Trends Neurosci. 38, 609–620. https://doi.org/10.1016/j.tins.2015.08.002.

Wright, D.K., Johnston, L.A., Kershaw, J., Ordidge, R., O'Brien, T.J., Shultz, S.R., 2017a. Changes in apparent fiber density and track-weighted imaging metrics in white matter following experimental traumatic brain injury. J. Neurotrauma 34, 2109–2118. https://doi.org/10.1089/neu.2016.4730.

Wright, D.K., O'Brien, T.J., Shultz, S.R., Mychasiuk, R., 2017b. Sex matters: repetitive mild traumatic brain injury in adolescent rats. Ann. Clin. Transl. Neurol. 4, 640–654. https://doi.org/10.1002/acn3.441.

Wright, D.K., Trezise, J., Kamnaksh, A., Bekdash, R., Johnston, L.A., Ordidge, R., Semple, B.D., Gardner, A.J., Stanwell, P., O 'brien, T.J., Agoston, D.V., Shultz, S.R., 2016. Behavioral, blood, and magnetic resonance imaging biomarkers of experimental mild traumatic brain injury. Sci. Rep. 6, 28713. https://doi.org/10.1038/srep28713.

Xiong, Y., Mahmood, A., Chopp, M., 2013. Animal models of traumatic brain injury. Nat. Rev. Neurosci. 14, 128–142. https://doi.org/10.1038/nrn3407.

Yu, F., Shukla, D.K., Armstrong, R.C., Marion, C.M., Radomski, K.L., Selwyn, R.G., Dardzinski, B.J., 2017. Repetitive model of mild traumatic brain injury produces cortical abnormalities detectable by magnetic resonance diffusion imaging, histopathology, and behavior. J. Neurotrauma 34, 1364–1381. https://doi.org/10.1089/neu.2016.4569.

Zhang, H., Schneider, T., Wheeler-Kingshott, C.A., Alexander, D.C., 2012. NODDI: practical in vivo neurite orientation dispersion and density imaging of the human brain. Neuroimage 61, 1000–1016. https://doi.org/10.1016/j.neuroimage.2012.03.072.

Zhao, J., Chen, Z., Xi, G., Keep, R.F., Hua, Y., 2014. Deferoxamine attenuates acute hydrocephalus after traumatic brain injury in rats. Transl. Stroke Res. 5, 586–594. https://doi.org/10.1007/s12975-014-0353-y.

Zhou, Y., 2017. Abnormal structural and functional hypothalamic connectivity in mild traumatic brain injury. J. Magn. Reson. Imaging 45, 1105–1112. https://doi.org/10.1002/jmri.25413.